INL/EXT-05-00785
Rev. 1

# AFC-1 Transmutation Fuels Post-Irradiation Hot Cell Examination 4 to 8 at.% Final Report

Irradiation Experiments
AFC-1B, AFC-1F and AFC-1Æ

Bruce Hilton
Douglas Porter
Steven Hayes

September 2006


The INL is a U.S. Department of Energy National Laboratory
operated by Battelle Energy Alliance

INL/EXT-05-00785
Rev. 1

# AFC-1 Transmutation Fuels Post-Irradiation Hot Cell Examination 4 to 8 at.% Final Report

**Irradiation Experiments**
**AFC-1B, AFC-1F and AFC-1Æ**

**Bruce Hilton**
**Douglas Porter**
**Steven Hayes**

**September 2006September 2006**

**Idaho National Laboratory**
**Idaho Falls, Idaho 83415**

**Prepared for the**
**U.S. Department of Energy**
**Office of Nuclear Energy**
**Under DOE Idaho Operations Office**
**Contract DE-AC07-05ID14517**

## CONTENTS

## LIST OF FIGURES

## LIST OF TABLES

## ABSTRACT

The AFC-1B, AFC-1F and AFC-1Æ irradiation tests are part of a series of test irradiations designed to evaluate the feasibility of the use of minor actinide bearing fuel forms in advanced fuel cycles for the transmutation of transuranic elements from nuclear waste. The tests were irradiated in the Idaho National Laboratory's (INL) Advanced Test Reactor (ATR) to an intermediate burnup of 4 to 8 at.% ($2.7 - 6.8 \times 10^{20}$ fiss/cm$^3$). The tests contain metallic and nitride fuel forms with non-fertile (i.e., no uranium) and low-fertile (i.e., uranium bearing) compositions. Results of postirradiation hot cell examinations of AFC-1 irradiation tests are reported for eleven metallic alloy transmutation fuel rodlets and five nitride transmutation fuel rodlets. Non-destructive examinations included visual examination, dimensional inspection, gamma scan analysis, and neutron radiography. Detailed examinations, including fission gas puncture and analysis, metallography / ceramography and isotopics and burnup analyses, were performed on five metallic alloy and three nitride transmutation fuels. Fuel performance of both metallic alloy and nitride fuel forms was best correlated with fission density as a burnup metric rather than at.% depletion. The actinide bearing transmutation metallic alloy compositions exhibit irradiation performance very similar to U-xPu-10Zr fuel at equivalent fission densities. The irradiation performance of nitride transmutation fuels was comparable to limited data published on mixed nitride systems.

# 1 INTRODUCTION

## 1.1 Background

The U. S. Advanced Fuel Cycle Initiative (AFCI) seeks to develop and demonstrate the technologies needed to transmute the long-lived transuranic actinide isotopes contained in spent nuclear fuel into shorter-lived fission products, thereby dramatically decreasing the volume of material requiring disposition and the long-term radiotoxicity and heat load of high-level waste sent to a geologic repository [Ref. 1, 2]. The AFC-1 irradiation tests are designed to evaluate the feasibility of the use of actinide bearing fuel forms in advanced fuel cycles for the transmutation of transuranic elements from nuclear waste [Refs. 3, 4]. AFC-1B, AFC-1F and AFC-1Æ are the first set of irradiation tests to be studied. AFC-1B and AFC-1F contain non-fertile and low-fertile actinide bearing metallic alloy fuel compositions. AFC-1Æ contains both non-fertile and low-fertile actinide bearing nitride fuel compositions. The tests were irradiated in the Idaho National Laboratory's (INL) Advanced Test Reactor (ATR) to an intermediate burnup of 4 to 8 at.% ($2.7 - 6.8 \times 10^{20}$ fiss/cm$^3$). Sibling tests are being irradiated to reach a final burnup of 30 to 40 at.% [Ref. 7].

The primary purpose of the post-irradiation examinations (PIE) is to characterize the feasibility and relative performance of metallic and nitride fuel forms for actinide transmutation advanced fuel cycles. The feasibility evaluation will support the Secretary of Energy's recommendation for the need of a second repository in the 2007-2010 timeframe. The secondary purpose is to provide safety data for these fuel forms to support FUTURIX-FTA irradiation test in the PHENIX fast reactor at Marcoule, France starting in 2007.

## 1.2 Scope and Conduct

Preliminary results of postirradiation hot cell examinations of AFC-1 irradiation tests are reported for eleven metallic alloy transmutation fuel rodlets and five nitride transmutation fuel rodlets. Non-destructive examinations included visual examination, dimensional inspection, gamma scan analysis, and neutron radiography. Detailed examinations including fission gas puncture and analysis, metallography / ceramography and isotopics and burnup analyses were performed on five metallic alloy and three nitride transmutation fuels.

The postirradiation examinations (PIE) were performed at the Idaho National Laboratory Materials and Fuels Complex (INL MFC). The PIE workscope was conducted at the Hot Fuel Examination Facility (HFEF) and Analytical Laboratory (AL) at MFC.

## 1.3 Organization of Report

The report is organized into seven sections. Section 1, the introduction, provides background and scope of this report. Section 2 presents the as-built condition of the fuel tests. Section 3 summarizes the results of the capsule assembly postirradiation examinations. Section 4 presents the PIE results of the metallic alloy transmutation fuels and Section 5 presents the PIE results of the nitride alloy transmutation fuels. Section 6 is a summary of the preliminary results. References are listed in Section 8.

## 2 IRRADIATION TEST DESCRIPTION

The AFC-1B. AFC-1F and AFC-1Æ irradiation tests were designed to provide irradiation performance data at intermediate burnups of 4 to 8 at.% on non-fertile and fertile actinide transmutation fuel forms containing plutonium, neptunium and americium isotopes [Refs. 3-6]. AFC-1B contains four non-fertile metallic fuel compositions (Pu-12Am-40Zr, Pu-10Am-10Np-40Zr, Pu-60Zr and Pu-40Zr). AFC-1F contains four fertile metallic fuel compositions (U-28Pu-4Am-2Np-30Zr, U-27Pu-3Am-2Np-40Zr, U-34Pu-4Am-2Np-20Zr, and U-29Pu-7Am). AFC-1Æ is a consolidation of the non-fertile and fertile nitride fuel compositions that were originally planned for Experiments AFC-1A and AFC-1E. AFC-1Æ contains two non-fertile nitride fuel compositions [$((Pu_{0.5},Am_{0.5})$N-36ZrN and $(Pu_{0.5},Am_{0.25},Np_{0.25})$N-36ZrN)] and one fertile nitride fuel composition [$((U_{0.5}Pu_{0.25},Am_{0.15},Np_{0.10})$N]. Figure 1 shows an example of metallic and nitride fuel specimens of one of the non-fertile actinide compositions that were fabricated for the AFCI Fuel Development Program. The fuel specimens are encapsulated in rodlet assemblies.

The rodlet assembly is designed as a miniature fast reactor fuel rod with a standard diameter and reduced length. The rodlet assembly consists of the metallic or nitride fuel column, sodium bond, stainless steel Type 421 (HT-9) cladding and an inert gas plenum. A stainless steel capsule assembly contains a vertical stack of six rodlet assemblies. The capsule and rodlet radial dimensions of the metallic and nitride fuel specimens are shown in Figure 2. The annular gap between the fuel column and rodlet inner diameter is initially filled by the sodium bond and is designed to accommodate fuel swelling during irradiation. The annular helium-filled gap between the rodlet outer diameter and capsule inner diameter is designed to provide the thermal resistance necessary to achieve the design irradiation temperature of the fuel specimen.

Figure 3 shows the fuel rodlet assembly axial dimensions for the metallic and nitride fuels. The design length of the metallic fuel column is 1.5-in. with the exception of the Pu-60Zr fuel composition which is 1.0-in.; the metallic fuel column may consist of a maximum of two pins, and the design diameter is 0.158-in. The design length of the nitride fuel column is 2.0-in. (consisting of seven to twelve pellets) and the design diameter is 0.168-in. The sodium bond is designed to exceed the fuel column length by 0.25 - 0.50-in. in length. The cladding for all rodlets is 6.0-in. in length (including welded endplugs) with 0.230-in. outer diameter and 0.194-in. inner diameter.

The irradiation test assembly consists of the experiment basket and one capsule assembly, which contains six rodlets. The irradiation test assembly, capsule assembly and rodlet assembly are shown in Figure 4. The experiment basket of the test assembly is designed to interface the capsule assembly with the ATR and to act as a thermal neutron flux filter. The capsule assemblies of the AFC-1B, -1Æ, and -1F irradiation tests are designated "B", "Æ" and "F", respectively. The rodlet assemblies are marked by unique serial numbers "(X)XX-XX(X)". The prefix characters designate the fuel composition of the rodlet, being labeled "AA" through "AE" for the non-fertile metallic alloys, "LAR" through "LAU" for the low-fertile metallic fuel alloys, "NM" and "NN", for the non-fertile nitride fuels and "LNX" and "LNY" for the non-fertile nitride fuels. The suffix (after the hyphen) characters of the rodlet serial number are the capsule identifier (i.e., 1, 2, 3, and 4) and the specimen identifier (i.e., A, B, C,...). In this report, a simplified

rodlet identification scheme is used. The rodlet assemblies are designated by a four character identification: the first two characters signify the experiment series, A1 for AFC-1, the third character signifies the irradiation test capsule and the fourth character signifies the rodlet's irradiation position, numbered from the top of the capsule assembly. Tables 1-3 summarize the as-fabricated conditions.

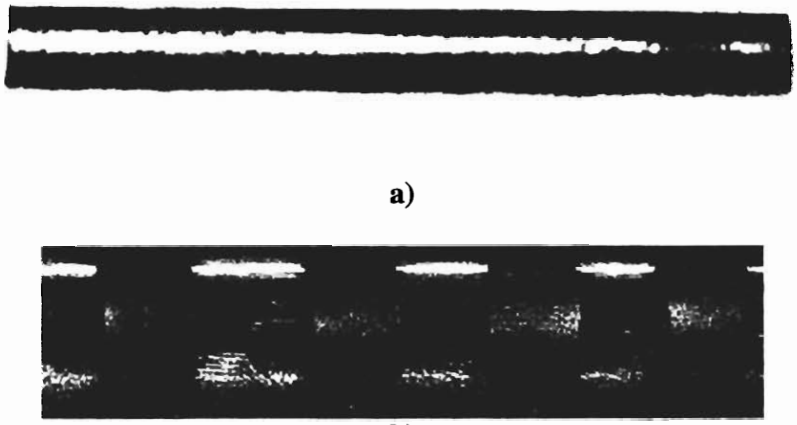

a)

b)

**Figure 1** AFC-1 non-fertile, minor actinide bearing fuel specimens a) metal alloy pin (Pu-12Am-40Zr) and b) nitride pellets ($Pu_{0.8}Am_{0.2}$)N-36ZrN

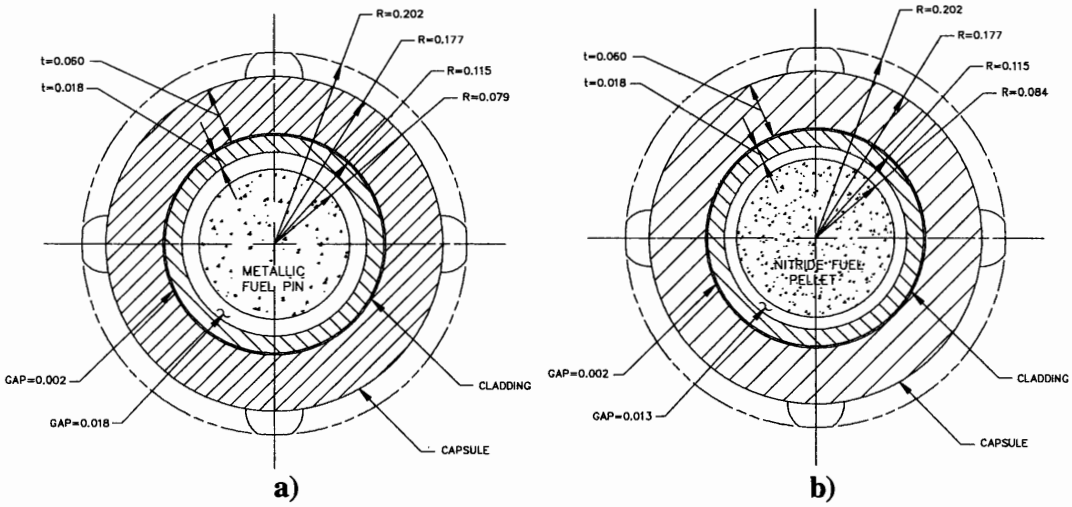


**Figure 2** Radial dimensions (inches) of capsule and fuel rodlet assemblies for a) metallic fuel and b) nitride fuel

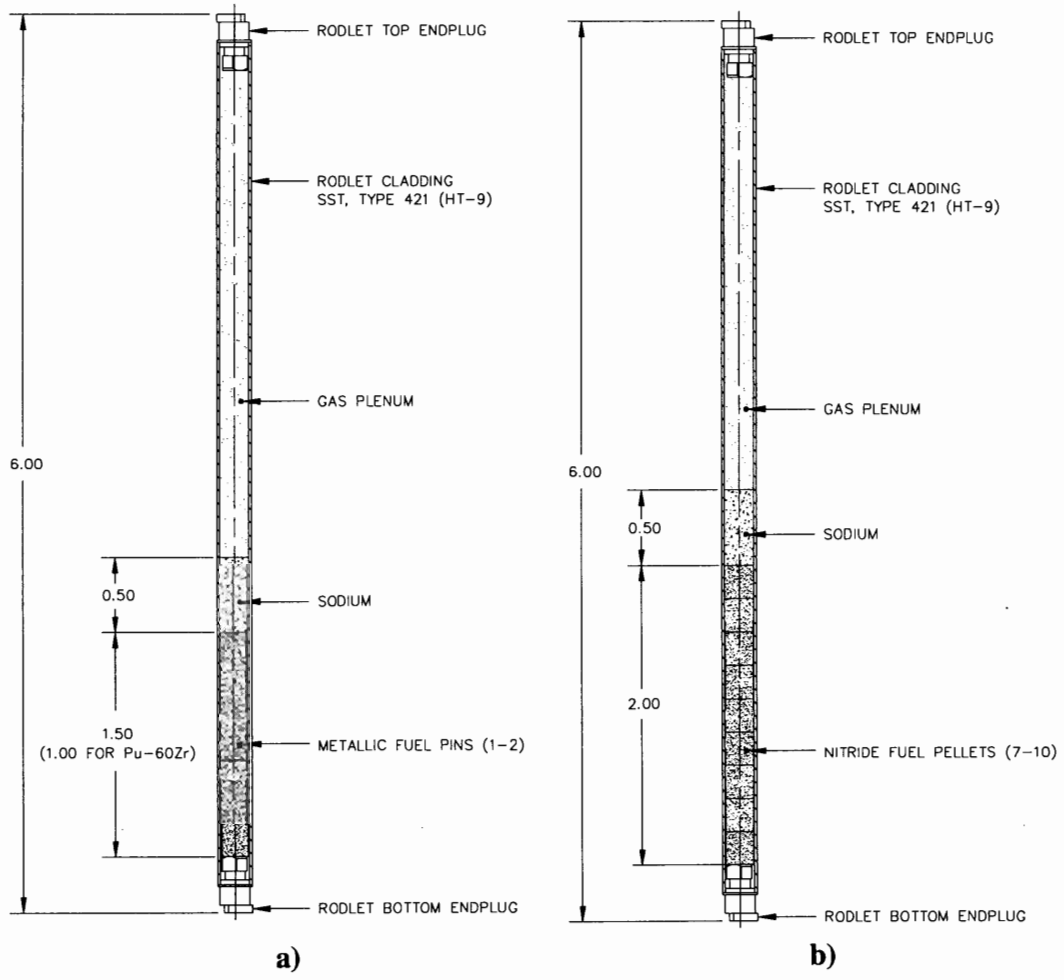


**Figure 3** Rodlet assembly axial dimensions (inches) for a) metallic fuel and b) nitride fuel

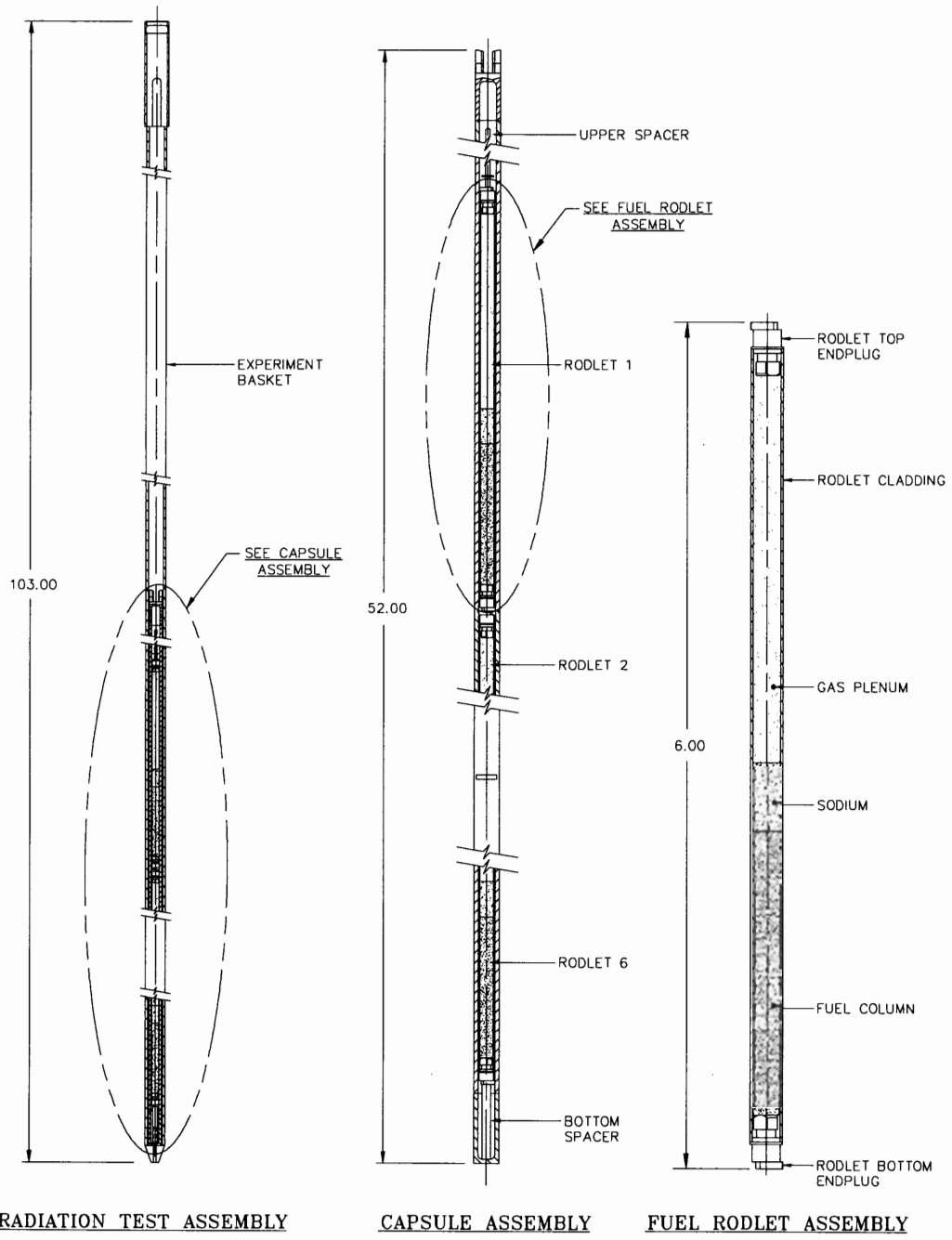


**Figure 4** AFC-1 irradiation test, capsule and rodlet assemblies (dimensions in inches)

**Table 1 AFC-1B Capsule As-Fabricated Conditions**

| Rodlet ID | A1B1 | A1B2 | A1B3 | A1B4 | A1B5 | A1B6 |
|---|---|---|---|---|---|---|
| Serial No. | AC-1Ba | AD-1A | AE-1A | AC-1A | AA-1Bc | DUM-1 |
| Rodlet Height (inches) | 5.998 | 6.001 | 6.000 | 6.000 | 6.000 | 6.004 |
| Rodlet OD Top Weld (inches) | 0.231 | 0.231 | 0.231 | 0.231 | 0.232 | 0.230 |
| Rodlet OD (inches) | 0.230 | 0.230 | 0.230 | 0.230 | 0.230 | 0.230 |
| Rodlet OD Lower Weld (inches) | 0.231 | 0.231 | 0.231 | 0.2315 | 0.231 | 0.231 |
| Fuel Column Height (inches) | 1.510 ±0.0005 | 1.480 ±0.0005 | 1.490 ±0.0005 | 1.522 ±0.001 | 0.991 ±0.0005 | NA |
| Fuel OD (inches) | 0.153 ±0.0005 | 0.153 ±0.0005 | 0.151 ±0.0005 | 0.152 ±0.001 | 0.152 ±0.0005 | NA |
| Fuel Mass (grams) | 4.292 ±0.0005 | 4.546 ±0.0005 | 4.509 ±0.0005 | 4.551 ±0.001 | 2.572 ±0.0005 | NA |
| Fuel Density (g/cc) | 9.352 | 10.172 | 10.083 | 9.880 | 8.482 | NA |
| Fuel Nominal Composition | Pu-12Am-40Zr | Pu-10Am-10Np-40Zr | Pu-40Zr | Pu-12Am-40Zr | Pu-60Zr | NA |
| U (wt%) | 0.00 | 0.00 | 0.00 | 0.00 | 0.00 | |
| Pu (wt%) | 48.83 | 40.13 | 59.11 | 48.48 | 39.67 | |
| Am (wt%) | 12.40 | 10.8 | 0.32 | 11.96 | 0.00 | |
| Np (wt%) | 0.23 | 9.50 | 0.00 | 0.27 | 0.00 | |
| Zr (wt%) | 41.00 | 41.00 | 41.00 | 40.80 | 60.70 | |
| N (wt%) | 0.00 | 0.00 | 0.00 | 0.00 | 0.00 | |
| C (wt%) | NM | NM | 0.008 | NM | 0.194 | |
| O (wt%) | NM | NM | 0.069 | NM | 0.020 | |
| Na Mass (grams) | 0.49 | 0.49 | 0.49 | 0.49 | 0.41 | NA |
| Rodlet Plenum Gas (mole%) | | | | | | |
| He | 27.19±1.4 | 36.3±0.3 | 36.3±0.3 | 36.3±0.3 | 23.64±1.2 | 14.96±0.8 |
| Ar | 72.2±0.7 | 62.55±0.6 | 62.55±0.6 | 62.55±0.6 | 75.72±3.8 | 83.85±0.8 |
| O2 | 0.01±.003 | 0.01±.003 | 0.01±.003 | 0.01±.003 | 0.01±.003 | 0.01±.003 |
| H2 | 0.02±.006 | 0.15±0.02 | 0.15±0.02 | 0.15±0.02 | 0.01±.003 | 0.54±0.05 |
| N2 | 0.59±0.09 | 0.48±0.05 | 0.48±0.05 | 0.48±0.05 | 0.58±0.06 | 0.64±0.06 |
| CO2 | 0.01±.003 | 0.01±.003 | 0.01±.003 | 0.01±.003 | 0.01±.003 | <0.01 |
| Capsule Fill Gas (mole%) | 99.88He, <0.01$O_2$, <0.01Ar, 0.06$N_2$, 0.01$CO_2$, 0.06$H_2$ | | | | | |

**Table 2 AFC-1F Capsule As-Fabricated Conditions**

| Rodlet ID | A1F1 | A1F2 | A1F3 | A1F4 | A1F5 | A1F6 |
|---|---|---|---|---|---|---|
| Serial No. | LAR-3B | LAS-3A | LAT-3A | LAR-3A | LAU-3A | LAT-3B |
| Rodlet Height (inches) | 5.997 | 5.998 | 5.998 | 6.000 | 6.000 | 5.999 |
| Rodlet OD Top Weld (inches) | 0.230 | 0.230 | 0.230 | 0.230 | 0.230 | 0.230 |
| Rodlet OD (inches) | 0.229 | 0.229 | 0.229 | 0.229 | 0.229 | 0.229 |
| Rodlet OD Lower Weld (inches) | 0.230 | 0.230 | 0.230 | 0.230 | 0.230 | 0.230 |
| Fuel Column Height (inches) | 1.195 | 1.259 | 1.495 | 1.093 | 1.295 | 1.538 |
| Fuel OD (inches) | 0.154 | 0.152 | 0.155 | 0.152 | 0.155 | 0.154 |
| Fuel Mass (grams) | 4.264 | 4.981 | 4.873 | 3.837 | 4.616 | 4.846 |
| Fuel Density (g/cc) | 11.626 | 13.122 | 10.627 | 11.440 | 11.415 | 10.426 |
| Fuel Nominal Composition | U-29Pu-4Am-2Np-30Zr | U-34Pu-4Am-2Np-20Zr | U-25Pu-3Am-2Np-40Zr | U-29Pu-4Am-2Np-30Zr | U-28Pu-7Am-30Zr | U-25Pu-3Am-2Np-40Zr |
| U (wt%) | 34.85 | 40.04 | 30.75 | 34.70 | 35.03 | 29.27 |
| Pu (wt%) | 29.43 | 34.21 | 25.11 | 28.28 | 28.65 | 25.02 |
| Am (wt%) | 3.69 | 4.08 | 2.33 | 3.59 | 5.37 | 2.80 |
| Np (wt%) | 2.28 | 2.03 | 1.91 | 2.07 | 0.16 | 2.12 |
| Zr (wt%) | 29.73 | 19.50 | 40.40 | 31.18 | 30.45 | 40.85 |
| N (wt%) | 0.00 | 0.00 | 0.00 | 0.00 | 0.00 | 0.00 |
| C (wt%) | 0.00 | 0.00 | 0.00 | 0.00 | 0.00 | 0.00 |
| O (wt%) | 0.00 | 0.00 | 0.00 | 0.00 | 0.00 | 0.00 |
| Na Mass (grams) | 0.43 | 0.49 | 0.48 | 0.42 | 0.44 | 0.50 |
| Rodlet Plenum Gas (mole%) | | | | | | |
| He | 27.95±1.4 | 27.95±1.4 | 27.95±1.4 | 27.95±1.4 | 27.95±1.4 | 27.95±1.4 |
| Ar | 71.79±3.6 | 71.79±3.6 | 71.79±3.6 | 71.79±3.6 | 71.79±3.6 | 71.79±3.6 |
| O2 | <0.01 | <0.01 | <0.01 | <0.01 | <0.01 | <0.01 |
| H2 | <0.01 | <0.01 | <0.01 | <0.01 | <0.01 | <0.01 |
| N2 | 0.26±0.04 | 0.26±0.04 | 0.26±0.04 | 0.26±0.04 | 0.26±0.04 | 0.26±0.04 |
| CO2 | 0.01±.003 | 0.01±.003 | 0.01±.003 | 0.01±.003 | 0.01±.003 | 0.01±.003 |
| Capsule Fill Gas (mole%) | 99.88He, <0.01$O_2$, <0.01Ar, 0.06$N_2$, 0.01$CO_2$, 0.06$H_2$ | | | | | |

**Table 3 AFC-1Æ Capsule As-Fabricated Conditions**

| Rodlet ID | A1Æ1 | A1Æ2 | A1Æ3 | A1Æ4 | A1Æ5 | A1Æ6 |
|---|---|---|---|---|---|---|
| Serial No. | NN-4B | DUM-1AE | NN-4A | NN-1Aa | NM-4A | LNX-4Ba |
| Rodlet Height (inches) | 5.997 | 5.998 | 5.998 | 6.000 | 6.000 | 5.999 |
| Rodlet OD Top Weld (inches) | 0.230 | 0.230 | 0.230 | 0.230 | 0.230 | 0.230 |
| Rodlet OD (inches) | 0.229 | 0.229 | 0.229 | 0.229 | 0.229 | 0.229 |
| Rodlet OD Lower Weld (inches) | 0.230 | 0.230 | 0.230 | 0.230 | 0.230 | 0.230 |
| Fuel Column Height (inches) | 1.955 | NA | 2.048 | 0.701 | 1.980 | 2.020 |
| Fuel OD (inches) | 0.161 | NA | 0.164 | 0.172 | 0.167 | 0.168 |
| Fuel Mass (grams) | 5.811 | NA | 6.105 | 2.000 | 5.698 | 8.041 |
| Fuel Density (g/cc) | 8.906 | NA | 8.628 | 7.445 | 8.003 | 11.005 |
| Fuel Nominal Composition | (Pu0.5, Am0.5)N-36ZrN | NA | (Pu0.5, Am0.5)N-36ZrN | (Pu0.5, Am0.5)N-36ZrN | (Pu0.5, Am0.25, Np0.25)N-36ZrN | (U0.5, Pu0.25, Am0.15, Np0.10)N |
| U (wt%) | 0.00 | | 0.00 | 0.00 | 0.00 | 48.60 |
| Pu (wt%) | 33.11 | | 31.74 | 33.30 | 31.68 | 24.79 |
| Am (wt%) | 23.00 | | 26.00 | 21.50 | 12.60 | 12.00 |
| Np (wt%) | 1.27 | | 1.12 | 0.85 | 12.20 | 8.00 |
| Zr (wt%) | 34.30 | | 33.50 | 34.70 | 33.10 | 0.20 |
| N (wt%) | 5.0 | | 5.2 | 5.25 | 5.7 | 4.3 |
| C (wt%) | 1.58 | | 1.54 | 2.00 | 1.33 | 0.28 |
| O (wt%) | 0.69 | | 0.81 | 2.00 | 0.77 | 0.36 |
| Na Mass (grams) | 0.479 | | 0.460 | 0.270 | 0.425 | 0.425 |
| Rodlet Plenum Gas (mole%) | | | | | | |
| He | 26.85 | 22.34 | 26.85 | 14.97 | 26.85 | 25.90 |
| Ar | 72.91 | 77.17 | 72.91 | 83.85 | 72.91 | 73.80 |
| O2 | 0.01 | 0.01 | 0.01 | 0.01 | 0.01 | 0.03 |
| H2 | 0.01 | 0.04 | 0.01 | 0.54 | 0.01 | 0.01 |
| N2 | 0.21 | 0.45 | 0.21 | 0.64 | 0.21 | 0.29 |
| CO2 | 0.01 | 0.01 | 0.01 | 0.01 | 0.01 | 0.01 |
| Capsule Fill Gas (mole%) | 99.66He, 0.01$O_2$, <0.01Ar, 0.14$N_2$, 0.02$CO_2$, 0.16$H_2$ | | | | | |

# 3 AFC-1B, AFC-1F AND AFC-1AE CAPSULE ASSEMBLY PIE

The preliminary results of post-irradiation hot cell examinations (PIE) of AFC-1B, AFC-1Æ, and AFC-1F Capsule Assemblies are presented in this section. Capsule visual examination and neutron radiography were used to evaluate the integrity of the capsules and rodlet assemblies and provide information for the disassembly process. The examination results are summarized and the capsule disassembly process is reported.

## 3.1 Capsule Visual Examination

AFC-1B, AFC-1F and AFC-1Æ irradiation tests were shipped from the INL Advanced Test Reactor (ATR) to INL Materials and Fuels Complex (MFC) in September 2004. Visual examination of the AFC-1 capsules was performed and documented using high resolution digital still camera (DSC) photography. Macrophotography through the cell-window and detailed inspections using a DSC coupled to a through-cell wall Kollmorgan periscope were completed.

The visual inspection of AFC-1B, AFC-1Æ and AFC-1F capsules concluded that there were no defects, pinholes, cracks or weld failures of the containers. The capsules were identified by the as-built markings electro-etched near the near the upper endcap in three positions spaced 120 degrees apart around the circumference. Inspection of the upper and bottom endcap welds at 10X magnification indicated no cracking, pinholes or degradation during irradiation (Figure 8). The general condition of the stainless steel capsule surface was shiny, similar to the pre-irradiation condition (Figures 5-7).

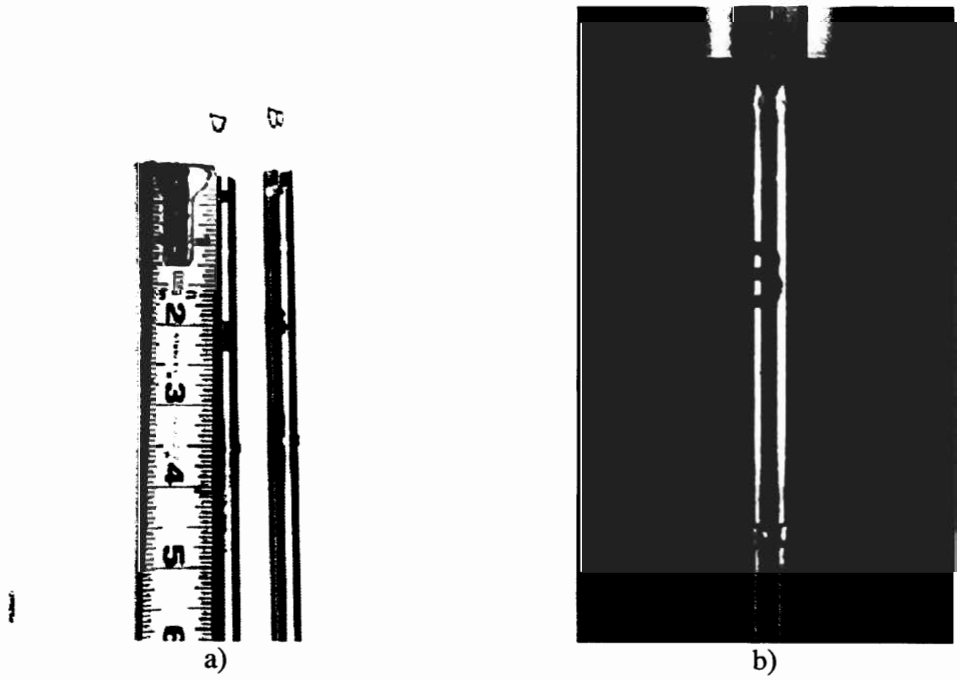


**Figure 5** Visual examination of AFC-1B Capsule Upper Endcap a) as-built and b) postirradiation

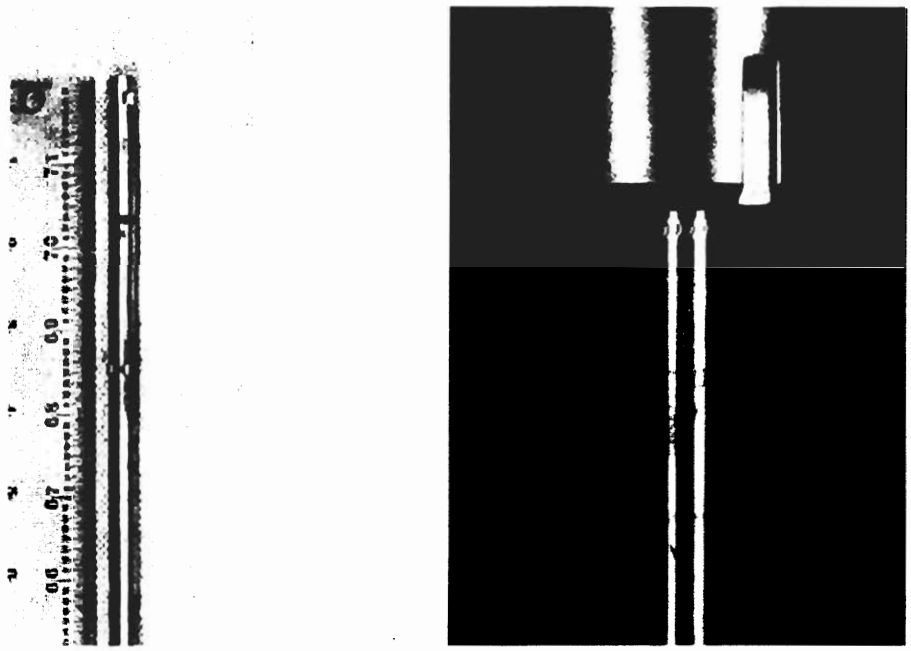

a) b)

**Figure 6** Visual examination of AFC-1F Capsule Upper Endcap a) as-built and b) postirradiation

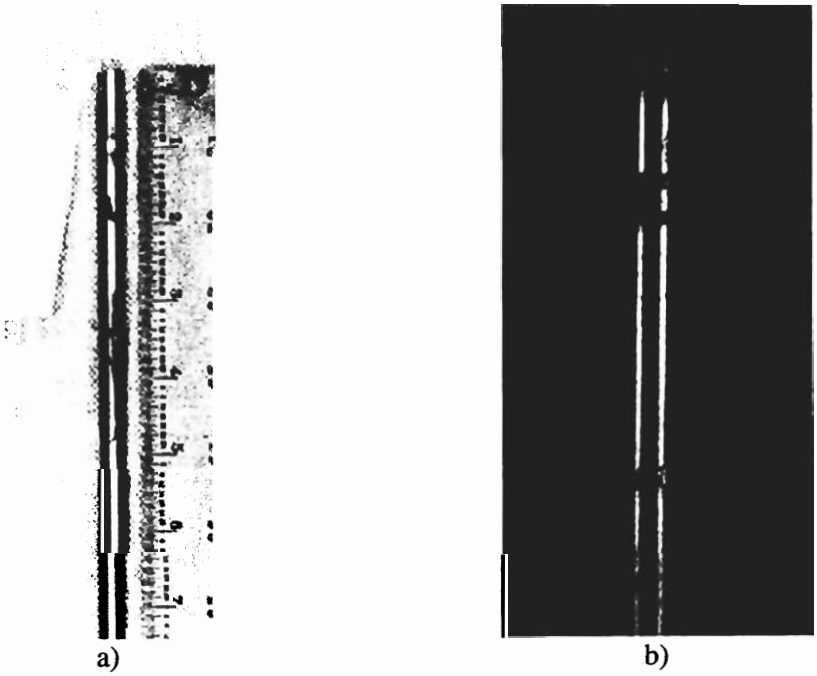

a) b)

**Figure 7** Visual examination of AFC-1Æ Capsule Upper Endcap a) as-built and b) postirradiation

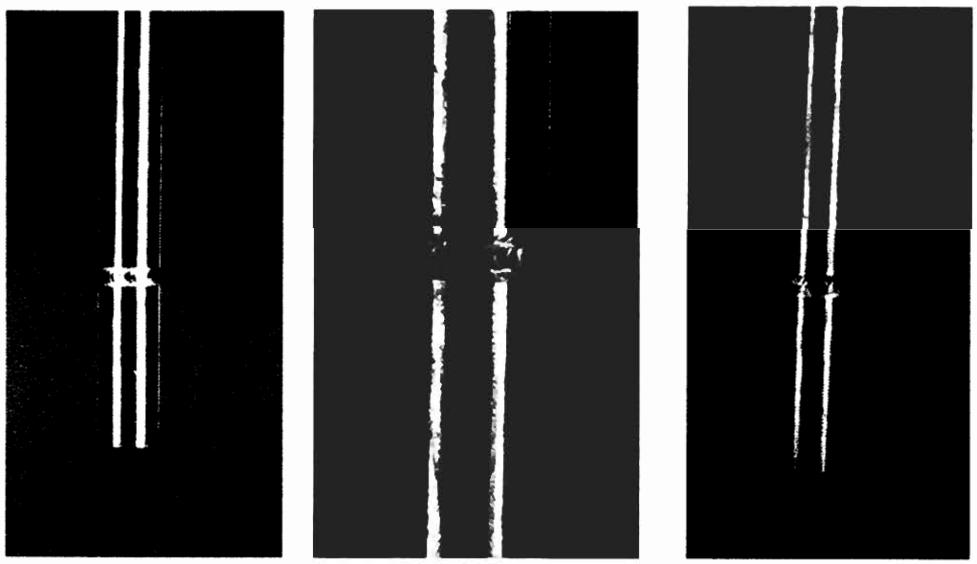

a) b) c)

**Figure 8** Visual examination of AFC-1 Capsule Bottom Endcap Welds for Capsule a) AFC-1B, b) AFC-1F, and c) AFC-1Æ

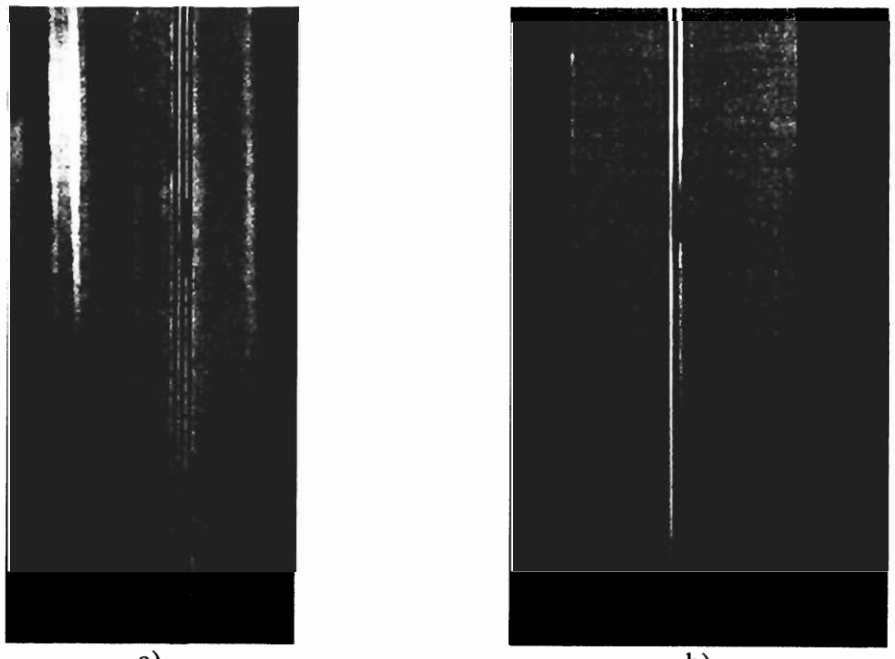

a) b)

**Figure 9** Surface discoloration of experiment capsules corresponding to fuel column axial positions of a) AFC-1B Capsule and b) AFC-1F Capsule

Figure 9 shows examination of regions of discoloration which corresponded to the axial positions of the fuel columns. There is no material concern associated with the discoloration. This type of discoloration is attributed to the heat flux and is similar to other capsule irradiation tests in the ATR.

### 3.2 Capsule Neutron Radiography

Neutron radiography of the capsules was used to examine the internal condition of the capsule assembly prior to removing the fuel rodlet assemblies. Neutron radiography was performed at INL MFC using the NRAD reactor (see Figure 10). Figure 11 shows photographs of the AFC-1 Irradiation Capsules neutron radiography. The neutron radiographs indicated no rodlet failures based on sodium and fuel column location. Sodium was not identified outside the rodlets which would occur in the event of a rodlet failure. The fuel columns show effects of irradiation, but did not exhibit significant changes in position or condition that would suggest a failure.

Other significant observations from capsule radiography are that nitride pellets revealed extensive cracking, but did not exhibit significant fragmentation caused by irradiation to this burnup. The susceptibility of transmutation nitride fuel to fragmentation is discussed further as part of nitride rodlet neutron radiography results Sec. 5. For the metallic alloys, the behavior appeared consistent with U-xPu-10Zr fuels. There is varying amounts of fuel axial growth and diameter increases indicative of fuel swelling.

Based on the capsule neutron radiography results, capsule disassembly was implemented as originally planned with sectioning upper and lower endcaps and sliding rodlets. Sectioning locations for capsule disassembly were identified from the radiographs and identification marks on the capsules.

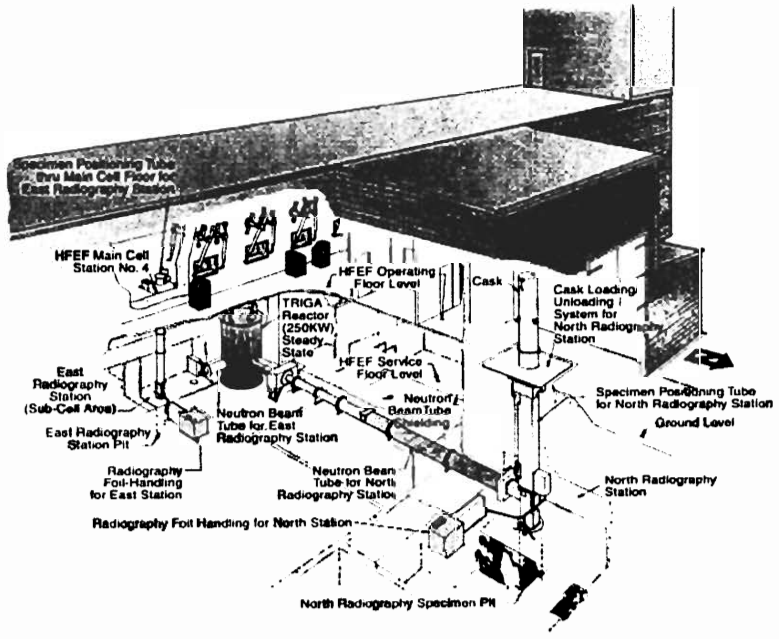


**Figure 10** Neutron radiography facility at INL MFC

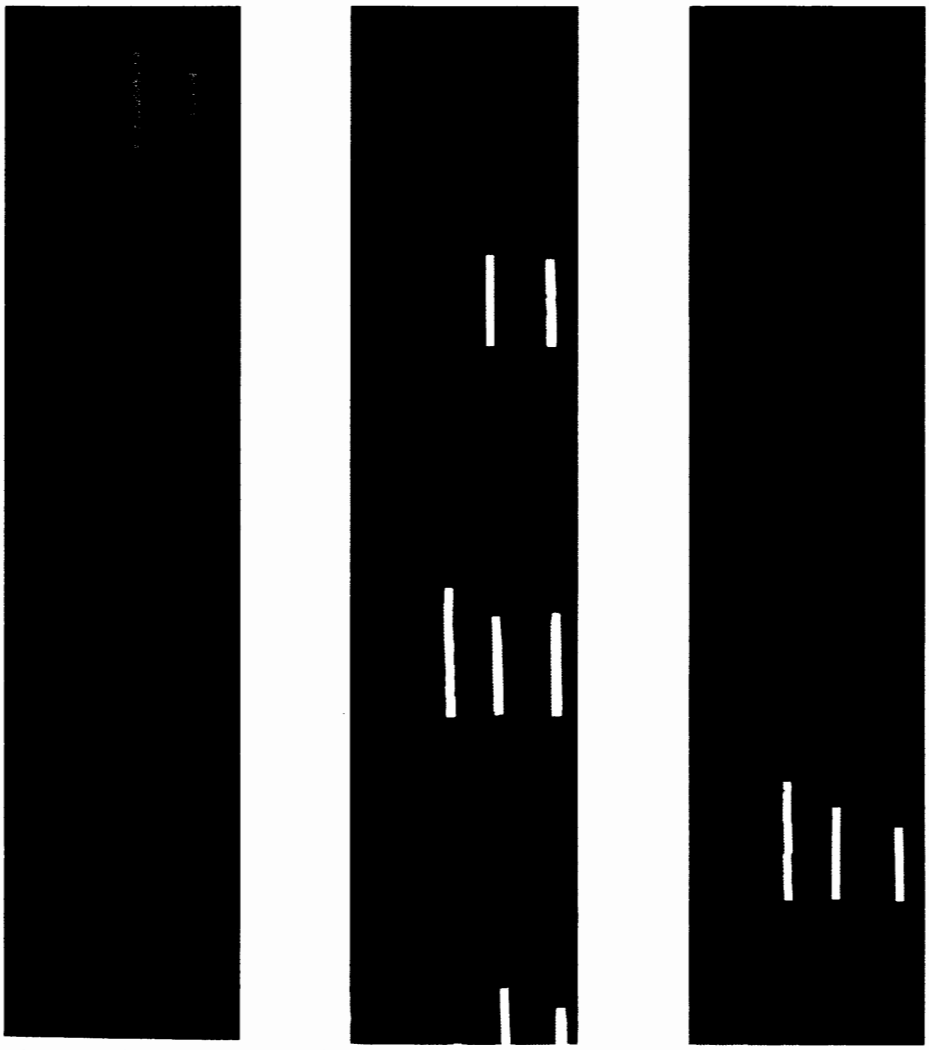


**Figure 11** Neutron radiography of AFC-1(Æ, B, F from left to right) Irradiation Capsules at three elevations a) 0 - 16 in., b) 14.5 - 31 in. and c) 29.5 - 46 in.

### 3.3 Capsule Disassembly

Capsule disassembly was performed using three methods after the capsule was sectioned at the top and bottom endcaps. First, the rodlets were removed one at a time using a push rod. This was successfully accomplished with three rodlets removed from Capsule Æ. They are A1Æ1, A1Æ2, and A1Æ6.

Since there was not a sufficient gap between the rodlet outer diameter and the capsule inner diameter to facilitate removal, the capsules were sectioned at positions corresponding to the rodlet interfaces. The as-fabricated interface positions were identified by the design drawings and capsule markings. The precise section positions were verified using results from the capsule neutron radiography.

Second, a Push Tool shown in Figure 12 was developed to increase leverage and apply force in a controlled manner to disassemble the remaining rodlets. The Push Tool was used on Rodlets A1Æ3, A1Æ4, A1Æ5 and A1B1. Attempts using the Push Tool were unsuccessful.

Third, an alternative disassembly milling technique was developed and implemented. A modified table top mill was retrofitted to accommodate the AFC-1 rodlets and qualified for disassembly. Figure 13 shows a schematic of the milling disassembly approach. The capsule wall was removed in two passes of 0.030 in. each, then the capsule rotated 180° and the capsule wall was removed again. Figure 14 shows the Disassembly Endmill apparatus during in-cell qualification. Milling depth was qualified to 0.0005 in. The potential for milling some of the rodlet cladding wall was identified, but deemed an acceptable risk since characterization of the cladding performance was not part of the AFC-1 workscope and further delays would jeopardize completion of the PIE workscope.

**Figure 12** Disassembly Push Tool

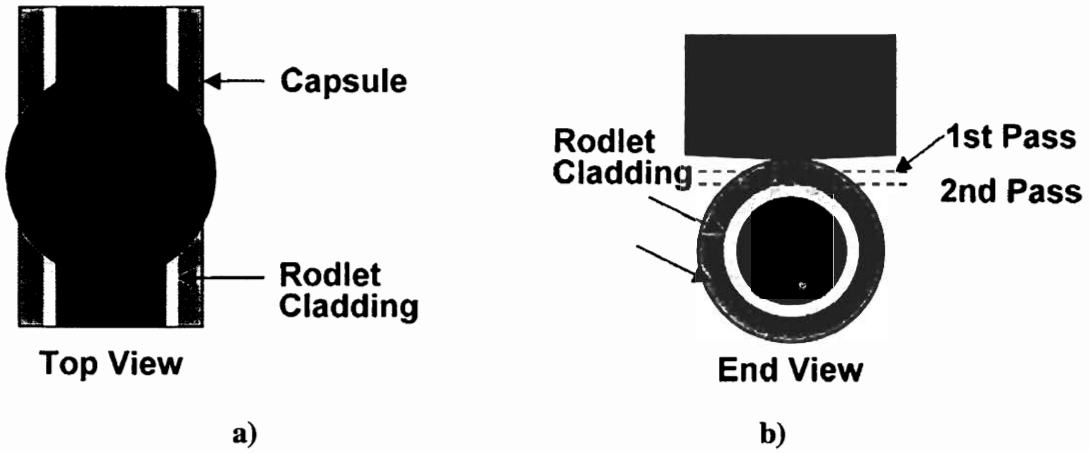


**Figure 13** Schematic of Endmill Disassembly Apparatus

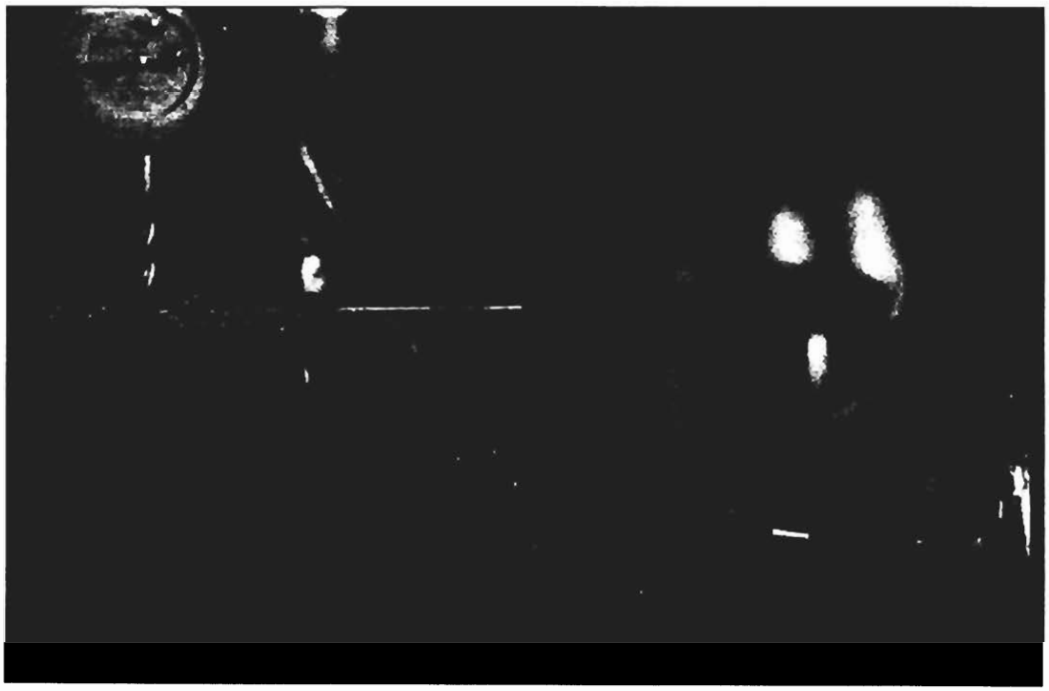

**Figure 14** Disassembly Endmill Apparatus during in-cell qualification

# 4 METALLIC ALLOY TRANSMUTATION FUELS PIE

The preliminary results of post-irradiation hot cell examinations (PIE) of metallic alloy transmutation fuel Experiments AFC-1B and AFC-1F are presented in this section. PIE of these irradiation fuel experiments provides irradiation performance data for non-fertile and fertile actinide-bearing metallic fuel compositions at an intermediate burnup of 4 to 8 at.%. Irradiation performance data at burnups up to 40 at.% will be obtained from sibling experiments that are currently being irradiated at the INL ATR. The PIE of the 40 at.% burnup metallic fuels is tentatively planned to begin in the first part of 2008.

These data support AFCI objectives to evaluate technical feasibility of metallic alloy transmutation fuel forms. The PIE data also support transmutation fuel testing in the FUTURIX-FTA irradiation experiment currently scheduled to commence in 2007.

## 4.1 Metallic Alloy Rodlet Visual Examination

The eleven metallic rodlet assemblies were visually examined after capsule disassembly to identify deviations from the as-built condition. The visual examinations revealed no deviations, cladding tube or end cap failures, deformations, cracks, blisters, areas of discoloration, corrosion, or loss of material by wear. Fig. 15 shows the digital still photographs of Rodlets A1B1 and A1F4 typical of the eleven metallic fuel rodlets.

a) b)

**Figure 15** Visual examination digital still photographs of transmutation metallic fuel rodlet assemblies a) A1B1 with Pu-12Am-40Zr fuel composition and b) A1F4 with U-29Pu-4Am-2Np-30Zr fuel composition

## 4.2 Metallic Alloy Rodlet Assembly Dimensional Inspections

Dimensional inspection of AFC-1B and AFC-1F Irradiation Test rodlets are summarized in this section. Eleven metallic alloy rodlets and one dummy rodlet from AFC-1B Capsule were inspected using INL Element Contact Profilometer (ECP). For each rodlet, four diameter profiles separated 45 degrees apart were measured at 0.1 in. intervals (2.54 mm) to an accuracy of ±0.0003 in. (7.6 $\mu$m). In general, the nominal diameter of the metallic rodlets was the same as the as-built dimensions. Fig. 16 shows a diameter profile of AC-1A as a typical example of the metallic rodlets.

The diameter profile of some of the rodlets exhibited effects of the disassembly milling operation. Some profiles had localized burrs that were manifest as isolated points with a larger diameter as shown in Figure 17. There were other rodlet profiles that revealed a slowly decreasing trend, which was interpreted as a decrease in cladding wall thickness caused by the disassembly milling.

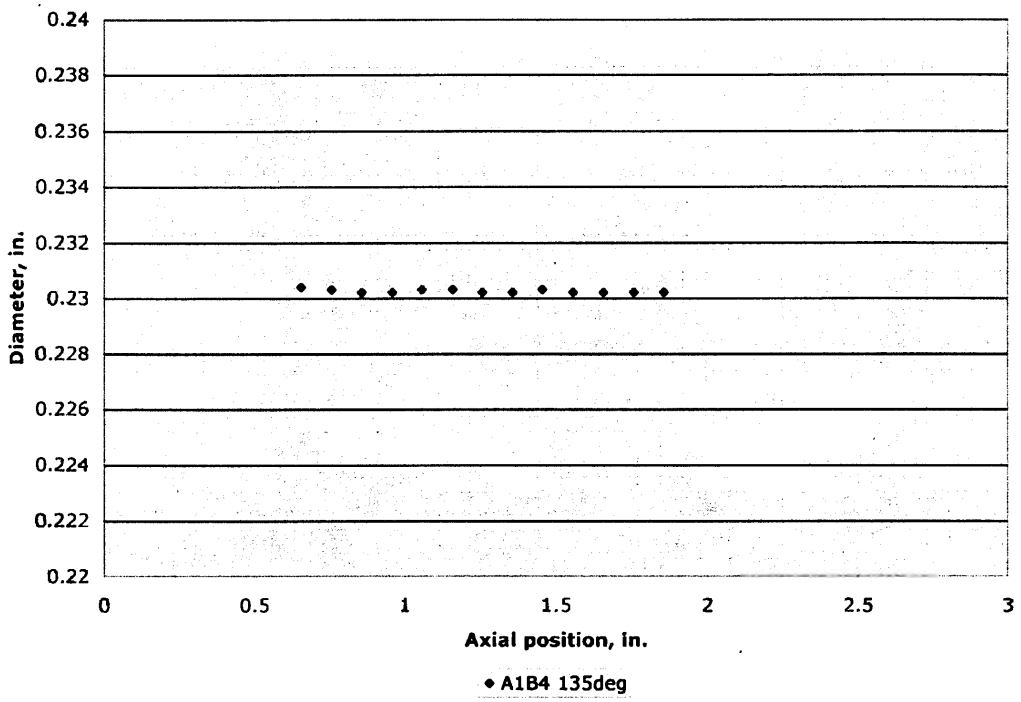


**Figure 16** Diameter profile of A1B4, Pu-12Am-40Zr, irradiated to 6.4 x $10^{20}$ f/cm$^3$ (6.8 at.%) burnup. Example of typical diameter profile nominally the same as as-built diameter of 0.230 in.

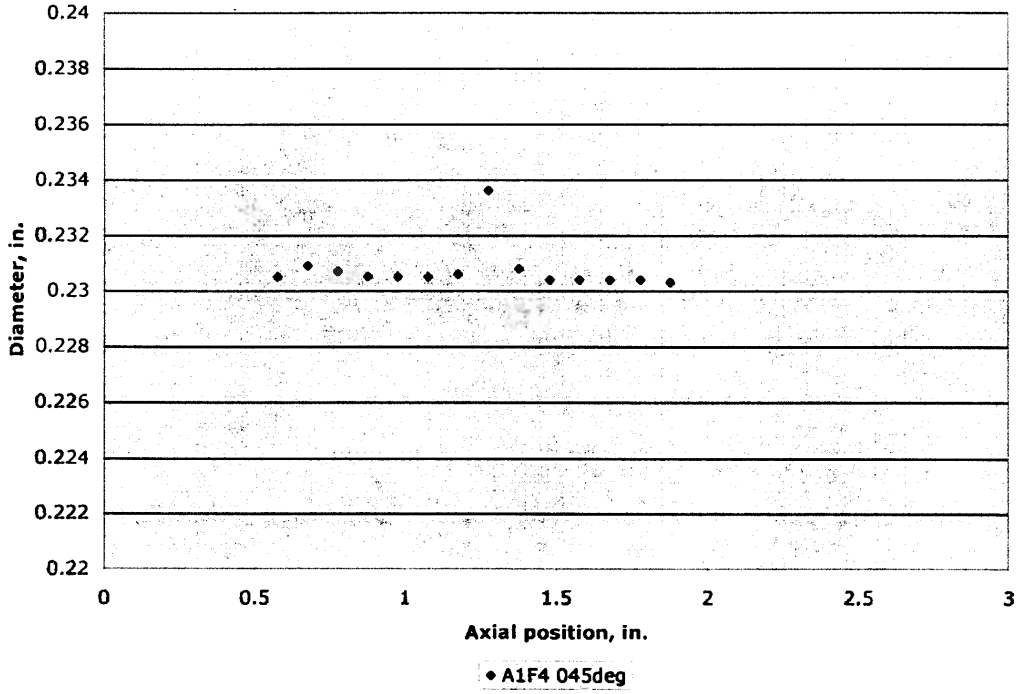


**Figure 17** Diameter profile of A1F4, U-29Pu-4Am-2Np-30Zr, irradiated to 8.9 x $10^{20}$ f/cm$^3$ (6.0 at.%) burnup. Example of localized burr effect due to disassembly milling operation (see isolated point at 1.3 in. axial position).

The mass of the metallic alloy fuel rodlet assemblies was measured after capsule disassembly. Table 4 displays the as-built and postirradiation mass of each rodlet. There are slight differences in some of the rodlets which are attributed to the loss of material that occurred during disassembly milling operation. The postirradiated mass of A1F2 (LAS-3A) and A1F3 (LAT-3A), which show an increase, are considered the same as the as-built masses since the difference is within the experimental uncertainty of the measurement. In summary, the results of the mass measurement are not definitive because of the effects of the disassembly process, but comparison of the as-built and postirradiated mass suggests that there were no fuel failures.

**Table 4 Mass of AFC-1B and AFC-1F Metallic Alloy Rodlets**

| Rodlet | Mass As-Built, g | Mass PIE, g | Difference[a], g |
|---|---|---|---|
| **AFC-1B Rodlets** | ±0.01 | ±0.001 | ±0.01 |
| A1B1 (AC-1Ba) | 15.77 | 15.751 | -0.019 |
| A1B2 (AD-1A) | 16.10 | 16.011 | -0.089 |
| A1B3 (AE-1A) | 16.10 | 16.046 | -0.054 |
| A1B4 (AC-1A) | 16.09 | 15.813 | -0.277 |
| A1B5 (AA-1Bc) | 13.96 | 13.912 | -0.048 |
| A1B6 (DUM-1) | 10.99 | 10.749 | -0.151 |
| | | | |
| **AFC-1F Rodlets** | | | |
| A1F1 (LAR-3A) | 15.67 | 15.047 | -0.623 |
| A1F2 (LAS-3A) | 16.47 | 16.476 | +0.006 |
| A1F3 (LAT-3A) | 16.31 | 16.321 | +0.011 |
| A1F4 (LAR-3B) | 15.21 | 15.209 | -0.001 |
| A1F5 (LAU-3A) | 15.99 | 15.956 | -0.034 |
| A1F6 (LAT-3B) | 16.31 | 16.113 | -0.197 |

a Disassembly milling operation removed some cladding material as evidenced by diameter profiles. The potential decrease in mass was not quantified.

### 4.3 Metallic Alloy Rodlet Neutron Radiography

Rodlet neutron radiography was performed on 11 metallic alloys and one dummy irradiated in the AFC-1B and AFC-1F capsules. Figures 18a) and 18b) show the rodlet neutron radiography of the five AFC-1B metallic alloy rodlets and one dummy rodlet and the six AFC-1F metallic alloy rodlets. AFC-1B Capsule consisted of non-fertile metallic alloy fuel forms and AFC-1F Capsule consisted of low-fertile metallic alloy fuel forms (see Sec. 2 for compositions). Four of the eleven metallic alloy rodlets were inverted during disassembly and in-cell storage. The inverted rodlets were A1B3 (AE-1A), A1B5 (AA-1Ac), A1F3 (LAT-3A) and A1B4 (LAR-3B). There was no obvious impact on the rodlets from the change in vertical orientation. This is consistent with sodium bonded

fuel rodlets since the sodium bond is expected to be solid at the hot cell conditions. The neutron radiography indicated that the fuel was in good condition with no fuel failures. Fuel swelling to contact with the cladding was observed in some of the rodlets (B- and F-Rodlets 3 and 4). However, there was little swelling evident in the rodlets that accumulated lower burnup (i.e., A1B1, A1B6, A1F1 and A1F6). This suggests that the transition burnup for swelling is between that accumulated by rodlets in the low and peak fission rate positions. The appropriate burnup unit for interpreting the fuel behavior is discussed.

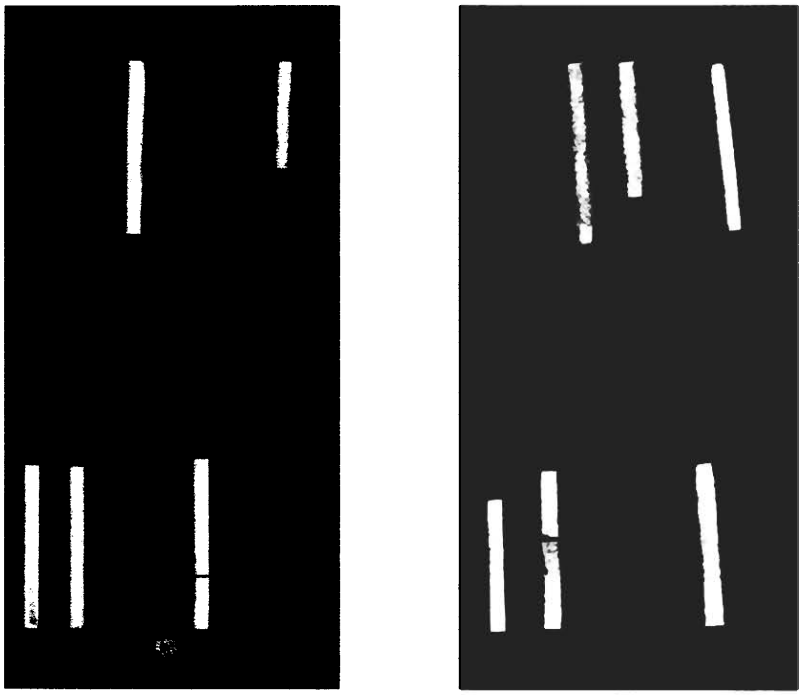

a) b)

**Figure 18** Rodlet neutron radiography of a) from l. to r., A1B1, A1B2, A1B3, A1B4, A1B5 and A1B6 b) from l. to r., A1F1, A1F2, A1F3, A1F4, A1F5, and A1F6

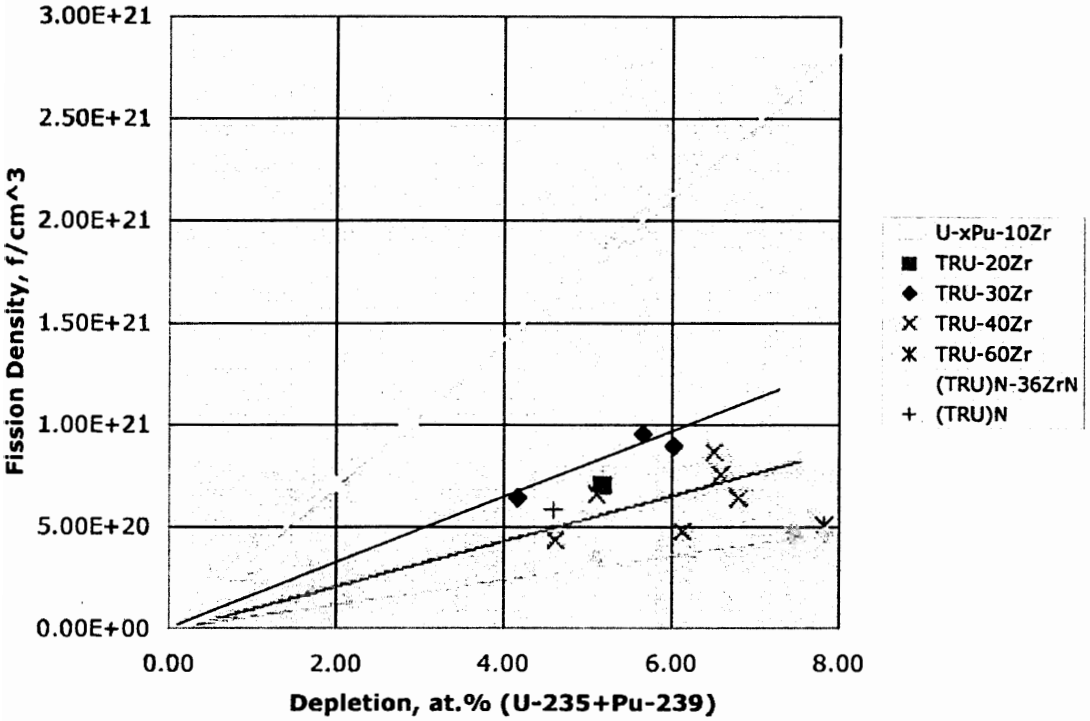


**Figure 19** Comparison of fission density and at.% depletion as burnup metrics for transmutation fuel forms

Typically at.% depletion or GWd/tU is used as a burnup metric, but the burnup metric that should be used to understand the transmutation fuel performance is fission density. Figure 19 shows the relationship of fission density and at.% depletion for the metallic and nitride transmutation fuel forms. The data for the metallic and nitride compositions are grouped by zirconium content. The burnup data for U-xPu-10Zr metallic fuel is also shown for comparison. The graph shows the proportional (or linear) relationship between fission density and at.% depletion and that the proportionality factor depends on fuel composition. More explicitly, the proportionality factor depends on the fissioning constituents density which is determined from the composition and the irradiation system's neutron spectrum. In a thermal neutron spectrum only fissile isotopes such as U-235, Pu-239, Pu-241 are included as fissioning constituents, however in a fast spectrum all the actinides are included as fissioning constituents.

Fig. 19 shows that the transmutation fuels have a much lower fission density than the U-xPu-10Zr at a particular at.% burnup. Using fission density as the burnup metric eliminates the composition dependence in assessing fission damage and provides a standard basis for correlating fuel performance parameters.

### 4.4 Metallic Alloy Rodlet Gamma Scan

Gamma scan analyses of AFC-1B and AFC-1F Irradiation Test rodlets are summarized in this section. Eleven metallic alloy rodlets and one dummy rodlet were analyzed for a number of fission products (Cs-134, Cs-137, Nb-95, Pr-144, Rh-106m, Ru-103, Zr-95) and activation products (Co-60, Mn-54). Figures 20-22 show five examples of the gamma scan results for actinide bearing metallic alloy fuels. There are two AFC-1B non-fertile metallic compositions (one at two burnup levels) and one AFC-1F fertile metallic composition at two burnup levels. At the top of each gamma scan graph is the neutron radiograph image to facilitate comparision between the fission product activity axial profile and internal rodlet features. The four isotopes displayed in each figure are representative of major fission product categories in the metal fuel system [Ref. 8]: 1. Nb-95, the elements in solution in the fuel, 2. Pr-144, the rare earths that generally precipitate as compounds or alloys , 3. Ru-103, the noble metals that precipitate as compounds, and 4. Cs-137, the alkali metals that dissolve to some extent in the bond sodium. Some general observations for all the metallic rodlets are provided. First, all the fission products, including cesium, generally map with the fuel location irrespective of the metallic alloy composition and burnup, which ranges from $3.5 - 6.8 \times 10^{20}$ f/cm$^3$. Second, the relative activity of the rodlets adjusted for decay time correspond approximately to fission density. Third, the lower activity axial positions often, but not always, correspond to a physical feature identified on the neutron radiograph such as a fuel pin interface or a lower density fuel region. Fourth, no fission product redistribution is evident at these burnups.

Considering the burnup level (based on fission density) of the transmutation metallic alloys, the gamma scan observations are consistent with the behavior of U-xPu-10Zr metallic fuels. The behavior of cesium activity demonstrates the importance of using fission density rather than at.% depletion as the burnup metric to understand the fuel performance. Figure 23 shows the development of the cesium activity profile of U-xPu-10Zr at three different burnups. The cesium initially maps with the fuel where it originates as a fission product, but during irradiation the cesium dissolves in the sodium as evidenced by the increased ratio of Cs in the sodium plug above the fuel column to the Cs in the fuel region. At $1.4 \times 10^{20}$ f/cm$^3$ (0.4 at.%) the ratio is zero and all the cesium is in the fuel. At $3.5 \times 10^{20}$ f/cm$^3$ (1 at.%) burnup, porosity has developed in the fuel sufficiently to allow the ratio between zero and one showing that some of the Cs has dissolved into the sodium. By $7.1 \times 10^{20}$ f/cm$^3$ (2 at.%) burnup, the ratio is ~2 and most of the Cs is dissolved in the sodium. Based on at.%, cesium activity of the AFC-1B and AFC-1F metallic alloy fuels is expected to map with the sodium. However, based on fission density, the cesium would still be in the fuel for most of the rodlets, which is the trend that was observed. In the 2 at.% profile, the gap between the top of the fuel column and the Cs activity peak is another interesting feature evident that was common in U-xPu-10Zr metallic fuel rods although not universally observed. This profile indicates that the sodium bond plug that is located on top of the fuel column is slightly displaced. The reason for the displacement is some fraction of the fission gas released from the fuel being trapped below the sodium plug; the trapped fission gas is contained in a volume such that the pressure above and below the sodium plug are balanced.

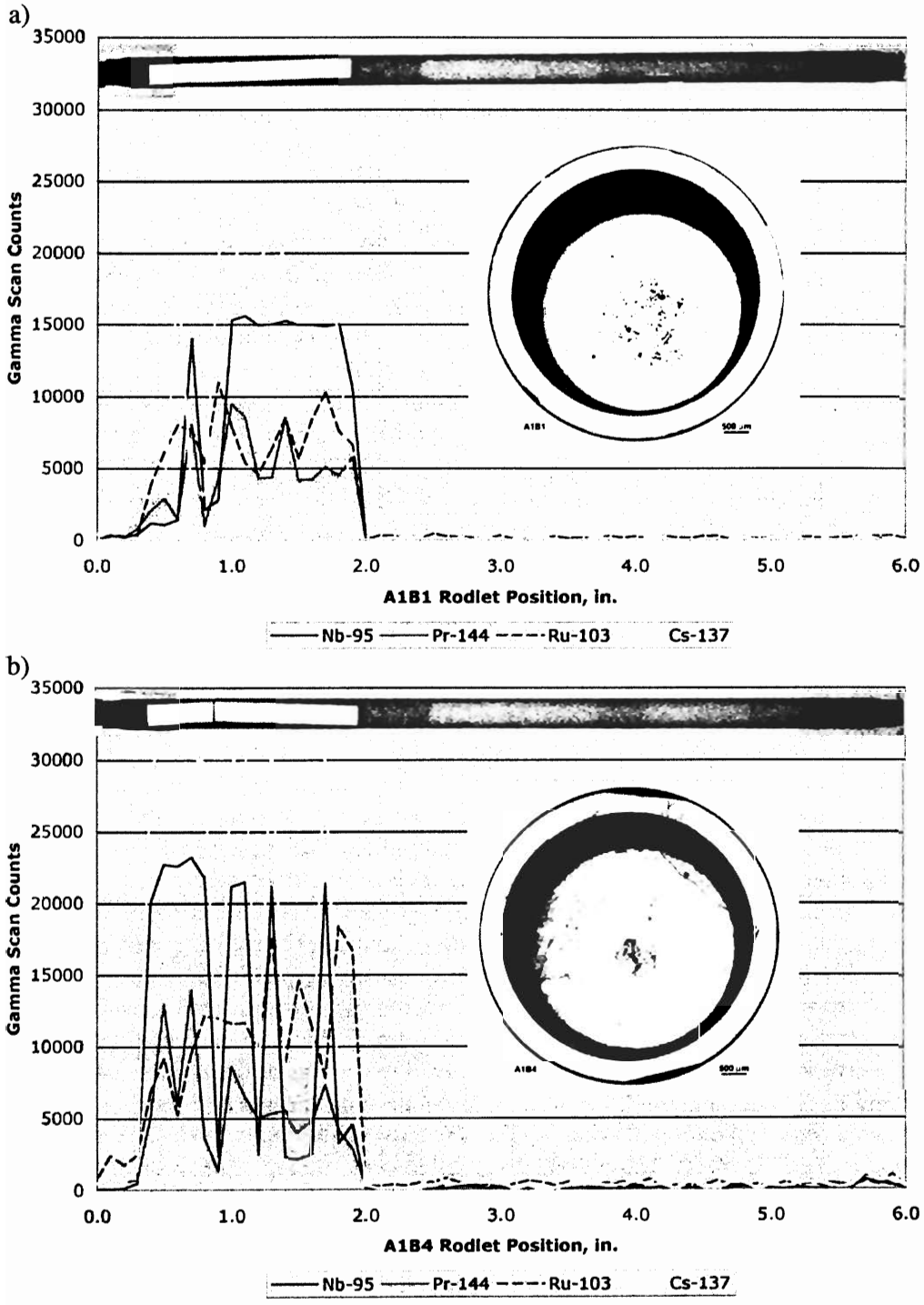


**Figure 20** Gamma scan analysis of Pu-12Am-40Zr compositions Pu-12Am-40Zr samples a) A1B1 (AC-1Ba) irradiated to 3.5 x $10^{20}$ f/cm$^3$ (4.6 at.%) burnup and b) A1B4 (AC-1A) irradiated to 4.7 x $10^{20}$ f/cm$^3$ (6.8 at.%) burnup

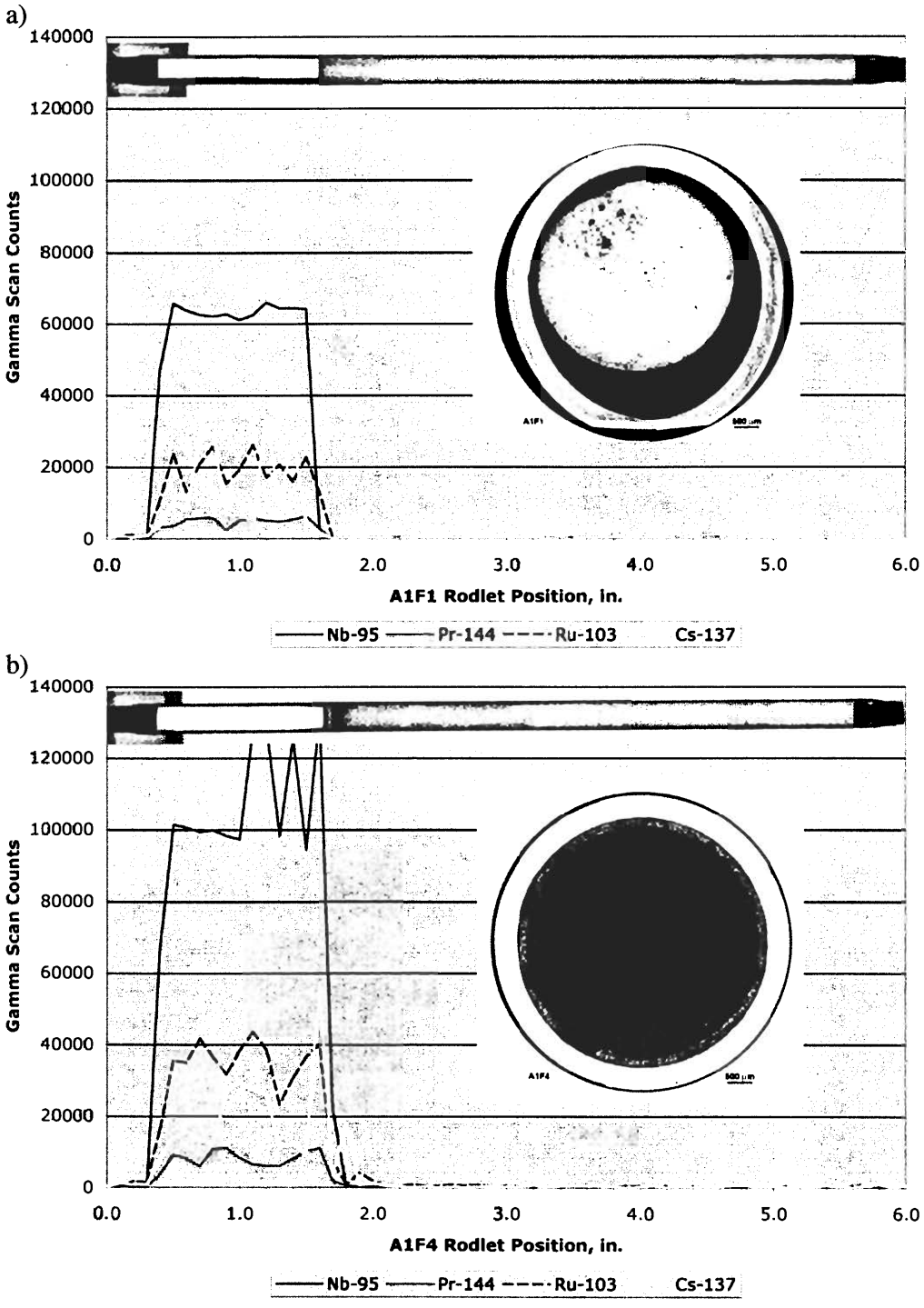


**Figure 21** Gamma scan analysis of U-29Pu-4Am-2Np-30Zr samples a) A1F1 (LAR-3A) irradiated to 5.0 x $10^{20}$ f/cm$^3$ (4.2 at.%) burnup and b) A1F4 (LAR-3B) irradiated to 6.8 x $10^{20}$ f/cm$^3$ (6.0 at.%) burnup

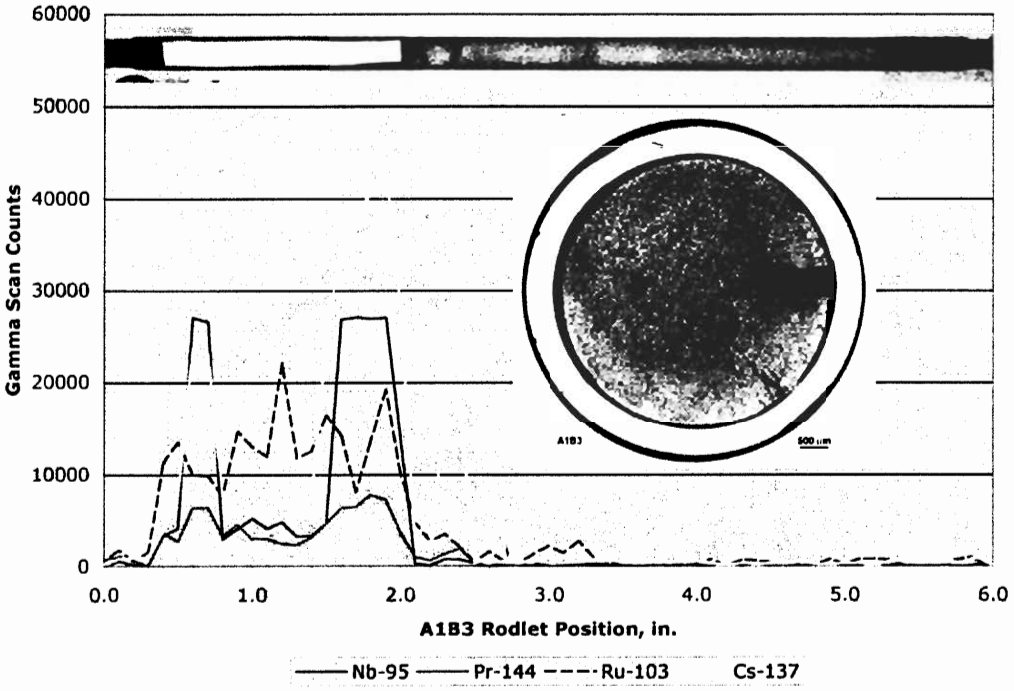


**Figure 22** Gamma scan analysis of Pu-40Zr sample A1B3 (AE-1A) irradiated to 6.1 x $10^{20}$ f/cm$^3$ (6.6 at.%) burnup

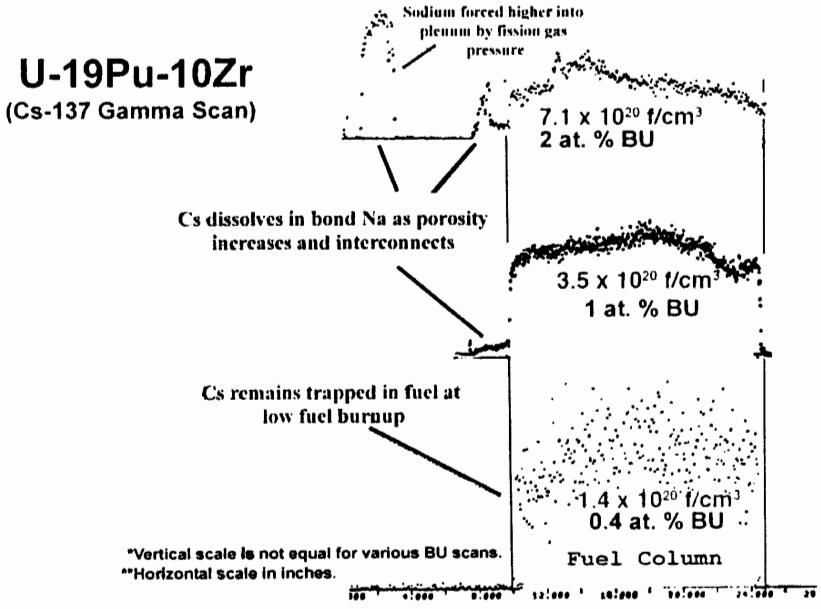


**Figure 23** Cesium fission product release typical of LMR metallic fuels [after Ref. 9]

## 4.5 Metallic Alloy Rodlet Fission Gas Puncture and Analyses

Fission gas samples were collected from the eleven metallic rodlet assemblies from AFC-1B and AFC-1F irradiation tests using the GASR laser puncturing and gas sampling system. The rodlet gas samples were analyzed for elemental and isotopic composition by gas mass spectrometry. Comparison of the elemental composition with as-built fill gas composition verified that there were no rodlet failures as was indicated by the visual and dimensional inspection results.

Fission gas and fractional helium release values were determined for each sample. The fission gas release was derived from the postirradiation and as-built elemental gas composition, the as-built rodlet internal void volume and internal gas pressure, and the fuel burnup. The fractional helium release was derived similarly from the postirradiation helium content, the as-built characterization data and the helium generation during irradiation. Helium generation was estimated to come only from americium transmutation.

Figure 24 displays the fission gas release burnup dependence of the 11 metallic alloy rodlets and includes data of U-xPu-10Zr for comparison. The fission gas release behavior of the transmutation metallic fuels follows the same trend as the U-xPu-10Zr fuel when correlated with fission density. There is negligible amount of fission gas release until a fission density of ~6.0 x $10^{20}$ f/cm$^3$. At this threshold burnup, there is a rapid increase in fission gas release displayed by the AFC-1 metallic fuel samples and is similar to U-xPu-10Zr behavior [Ref. 10]. It is significant that there is no difference in fission gas release behavior between the non-fertile (non-uranium bearing) and low-fertile (uranium bearing) compositions. Based on the observation that gas release behavior of the transmutation metallic alloys is similar to U-xPu-10Zr at this intermediate burnup, the fission gas release at higher burnup is predicted to show a slightly increasing trend. This will be evaluated during PIE of the sibling experiments AFC-1D and AFC-1H.

The axial growth, helium release behavior and fission gas release of the metallic rodlets irradiated in Capsule B and F are shown in Figures 25 and 26. All three parameters trend together. The axial growth percent is slightly higher than observed for U-xPu-10Zr fuel [Ref. 10] for which there are a number of possible explanations. First, this may be due to the lower smear density of the AFC-1 test rodlets, which would delay the time to fuel-cladding contact which restrains further axial growth due to friction forces. Second, a previously observed increased swelling at the top of the column (unrestrained) also may bias shorter fuel columns to appear to have higher uniform axial growth. Third, the lower peak fuel temperature of the AFC-1 Experiments compared to EBR-II operating conditions may also contribute to the higher axial growth since U-xPu-10Zr alloys axial growth was observed to be quite sensitive to temperature [Ref. 12]. The helium release follows the same trend as fission gas release, but is somewhat lower. Helium release rates are 0-15% compared to 0-36% fission gas release. At higher burnups, the helium release fraction is expected to be similar to fission gas. This will be evaluated during PIE of the sibling test, AFC-1H.

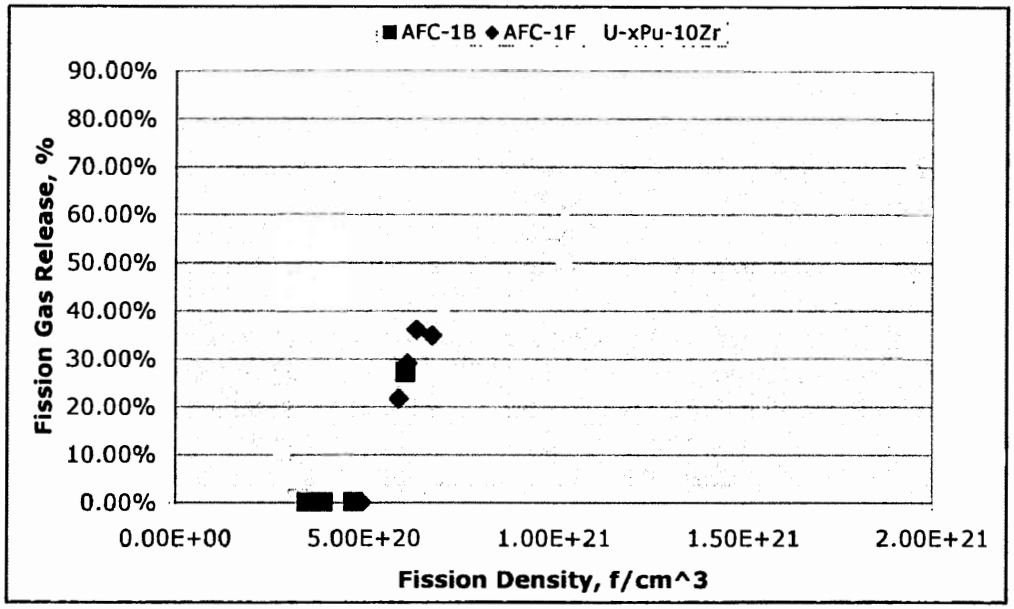


**Figure 24** Fission gas release from metallic alloy transmutation fuel rodlets irradiated in AFC-1B and AFC-1F Capsules and U-xPu-10Zr (Ref. 10)

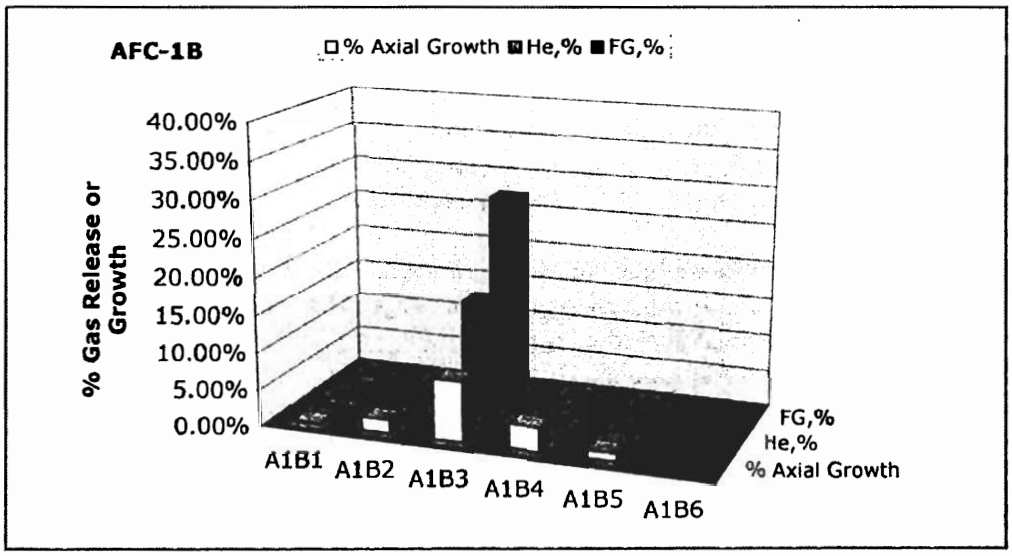


**Figure 25** Axial growth, helium release and fission gas release from metallic alloy transmutation fuel rodlets irradiated in AFC-1B Capsule

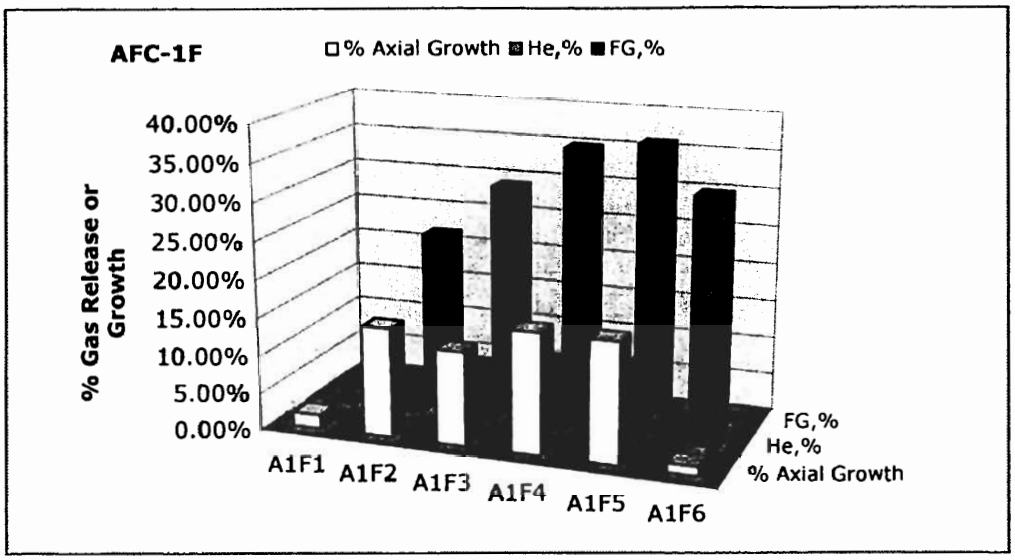


**Figure 26** Axial growth, helium release and fission gas release from metallic alloy transmutation fuel rodlets irradiated in AFC-1F Capsule

### 4.6 Metallic Alloy Rodlet Sectioning

Cross sectional (transverse) samples for isotopic and burnup analyses and metallography were sectioned from AFC-1B and AFC-1F fuel specimens. The sectioning location of the isotopic samples was 0.25 – 0.50 in. from the bottom of the rodlets and the sectioning location of the metallography samples was 0.50 – 0.75 in. from the bottom of the rodlets.

### 4.7 Metallic Alloy Metallography

Metallography results of AFC-1B and AFC-1F eleven metallic alloy samples are presented. All specimens were examined in the as-polished condition. In addition, six fertile metallic specimens were examined after etching with a 10% nitric acid- 10% hydrogen peroxide solution. Specimens A1B1, A1B4, A1F1 and A1F4 are compositions that will be tested in the FUTURIX-FTA Irradiation Test. Montage (or composite) overviews of the transverse cross sections were created from 12-16 images taken at 5X objective magnification. Detailed metallography was performed at magnifications up to ~500X. There were some samples that exhibited slight rounding at the highest magnification.

Figures 27 and 28 show the cross-sectional metallography of the AFC-1B and AFC-1F specimens as-polished. Only A1B3 of the AFC-1B specimens exhibits significant radial swelling. Of the AFC-1F specimens, four of the six specimens (A1F2, A1F3, A1F4, and A1F5) are fully swelled in contact with the cladding. The specimens that exhibit significant swelling also have fully developed porosity and indications of the beginning stages of zone formation. Zone formation in U-xPu-10Zr fuel is due to irradiation induced fuel constituent radial redistribution [Ref. 11]. Four non-fertile specimens (A1B1, A1B2, A1B4 and A1B5) and two fertile specimens (A1F1 and A1F6)

show the initial development stages of a distributed porosity and slight areal swelling, being typical features of metallic alloy fuels before transition [Ref. 11]. Figure 29 shows cross-sectional metallography of AFC-1F specimens after etching. Etching further revealed the porosity network, zone formation and microstructural features.

Figures 30-31 are higher magnification photomicrographs of the Pu-12Am-40Zr specimens (A1B1, A1B4) at the interior and edge regions. The interior appears homogeneous, containing a matrix phase with a high density of small pores and a secondary phase. The micrograph of A1B4 shows a mottled appearance in the interior. This is attributed to compositional variations based on similar microstructure that is observed in the as-cast specimens [Ref. 13]. which correlates with compositionbased on contrast differences. , a multi minor phase a multi-phase edge shows In the edge region there is a rim 100-150 $\mu$m wide, which has very little pores and a 10-20 $\mu$m outer layer or rind. Both of these features are observed in the as-cast microstructure.

Figures 32 and 33 display the higher magnification photomicrographs of U-29Pu-4Am-2Np-30Zr specimens as-polished and after etching. In A1F1, etching reveals details of the rim region and possibly a third intermediate region between the rim and interior. While etching results in different contrast zones in slightly swelled and fully swelled samples, it was somewhat less effective in providing additional information for the highly swelled samples at higher magnification (Figure 33b). The same features identified in A1B1 and A1B4 are also observed in A1F1 and A1F4. A1F4 is fully swelled, but still reveals a rim region 100-150 $\mu$m based on contrast difference in the as-polished photomicrograph. A1F4 is typical of the fully swelled specimens and shows a spongy microstructure with larger diameter pores in the interior and an annulus of slightly larger pores or annulur void region between the rim and interior.

The different swelling behavior and microstructure development of the AFC-1B and AFC-1F specimens is explained in terms of irradiation damage as correlated by fission density. This highlights the importance of using fission density rather than at.% burnup as the fission damage metric for fuels with varying compositions. Historically and particularly for metallic fuels, irradiation performance has been correlated to at.% burnup. This was a convenient and applicable metric for U-xPu-10Zr fuels since the zirconium content was a constant 10 wt.% and substituting plutonium for uranium did not significantly change the number of fissions in the fast neutron spectrum irradiations. However, in the AFC-1 tests, the zirconium ranges from 20 to 40 wt.% and the varying amounts of uranium and plutonium (specifically the U-235 and Pu-239 isotopes) have a significant effect on number of fissions in the ATR thermal neutron spectrum irradiations. To highlight the inappropriateness of using at.% burnup as a fission damage metric, we can evaluate A1B4 and A1F4. Based on at.% burnup, A1B4 (Pu-12Am-40Zr) with 6.8 at.% would be expected to have greater fission damage (and concomitantly more swelling) than A1F4 (U-29Pu-4Am-2Np-30Zr), with 6.0 at.%. Contrary to this A1B4 exhibited little swelling while A1F4 was fully swelled. The apparent inconsistent dependence between swelling and burnup based on at.% is eliminated when using fission density. A1F4 fission density is 6.8 x $10^{20}$ f/cm$^3$ which is 40% higher than A1B4 fission density of 4.7 x $10^{20}$ f/cm$^3$, thus the greater swelling is expected.

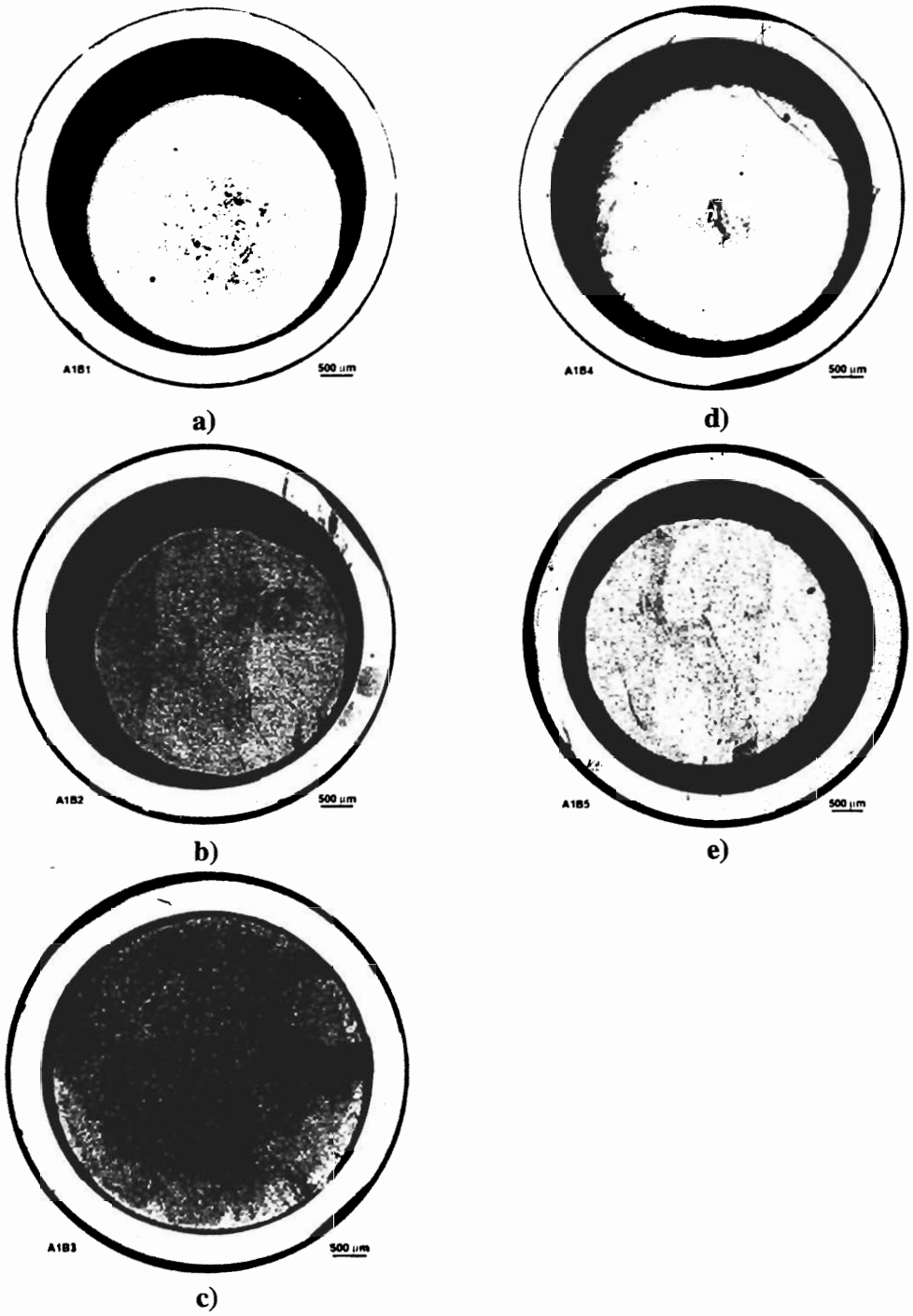


**Figure 27** Cross-sectional metallography of AFC-1B metallic non-fertile samples as-polished a) A1B1 irradiated to 3.5 x $10^{20}$ f/cm$^3$ (4.6 at.%), b) A1B2 irradiated to 3.9 x $10^{20}$ f/cm$^3$ (6.1 at.%), c) A1B3 irradiated to 6.1 x $10^{20}$ f/cm$^3$ (6.6 at.%) d) A1B4 irradiated to 4.7 x $10^{20}$ f/cm$^3$ (6.8 at.%) and e) A1B5 irradiated to 3.8 x $10^{20}$ f/cm$^3$ (7.8 at.%)

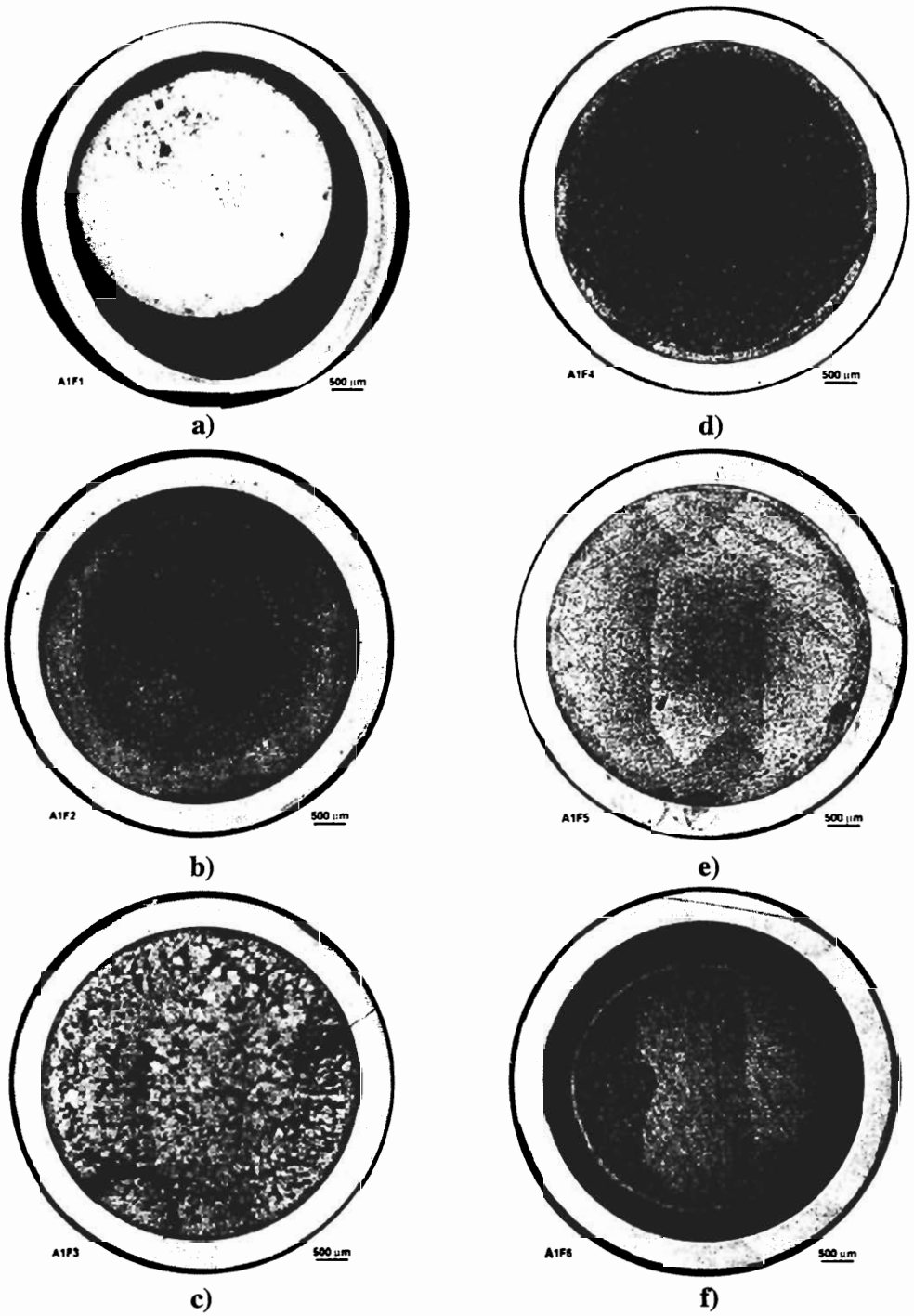


**Figure 28** Cross-sectional metallography of AFC-1F metallic fertile specimens as-polished a) A1F1 irradiated to 5.0 x $10^{20}$ f/cm$^3$ (4.2 at.%), b) A1F2 irradiated to 5.9 x $10^{20}$ f/cm$^3$ (5.2 at.%), c) A1F3 irradiated to 6.1 x $10^{20}$ f/cm$^3$ (6.5 at.%) d) A1F4 irradiated to 6.8 x $10^{20}$ f/cm$^3$ (6.0 at.%), e) A1F5 irradiated to 6.4 x $10^{20}$ f/cm$^3$ (5.7 at.%) and e) A1F6 irradiated to 4.8 x $10^{20}$ f/cm$^3$ (5.1 at.%)

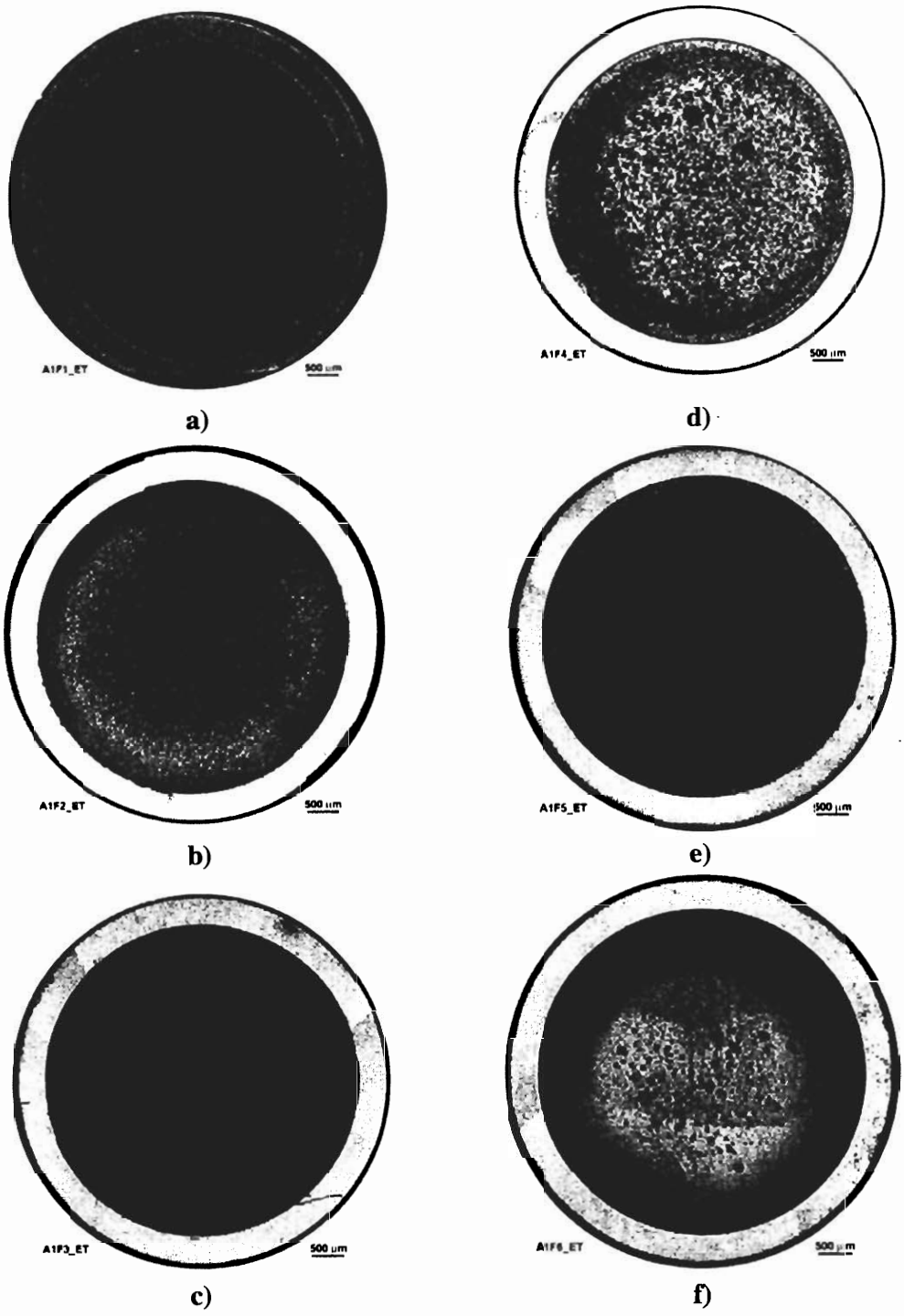


**Figure 29** Cross-sectional metallography of AFC-1F metallic fertile specimens etched a) A1F1 irradiated to 5.0 x $10^{20}$ f/cm$^3$ (4.2 at.%), b) A1F2 irradiated to 5.9 x $10^{20}$ f/cm$^3$ (5.2 at.%), c) A1F3 irradiated to 6.1 x $10^{20}$ f/cm$^3$ (6.5 at.%) d) A1F4 irradiated to 6.8 x $10^{20}$ f/cm$^3$ (6.0 at.%), e) A1F5 irradiated to 6.4 x $10^{20}$ f/cm$^3$ (5.7 at.%) and e) A1F6 irradiated to 4.8 x $10^{20}$ f/cm$^3$ (5.1 at.%)

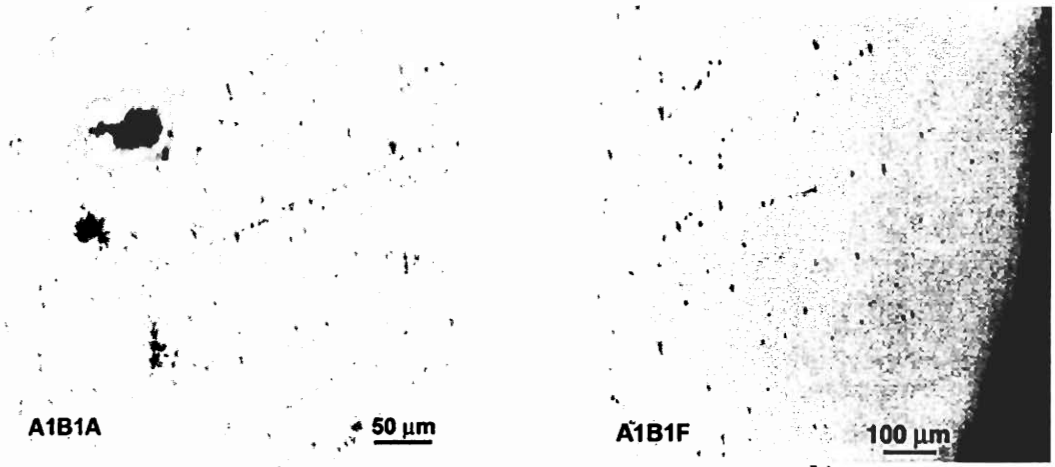


a) b)

**Figure 30** Optical micrographs of A1B1 as-polished a) interior and b) edge region

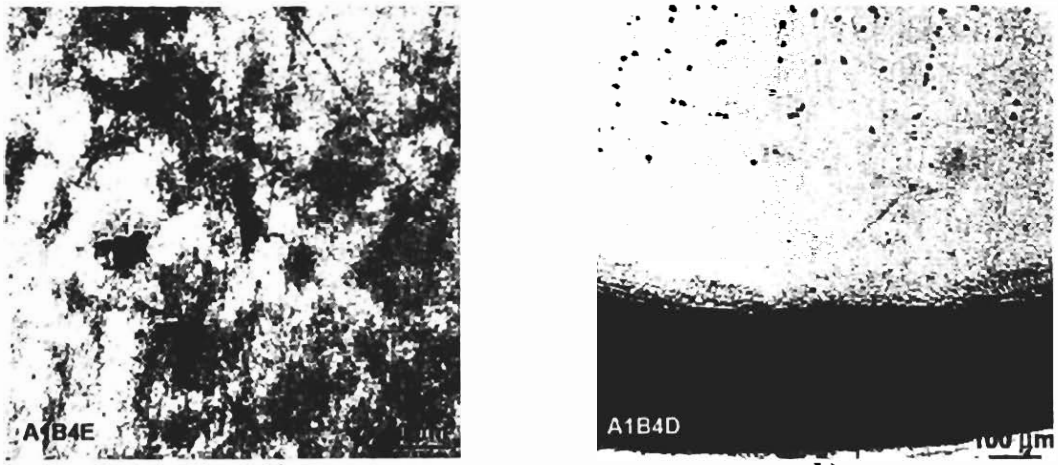


a) b)

**Figure 31** Optical micrographs of A1B4 as-polished a) interior and b) edge region

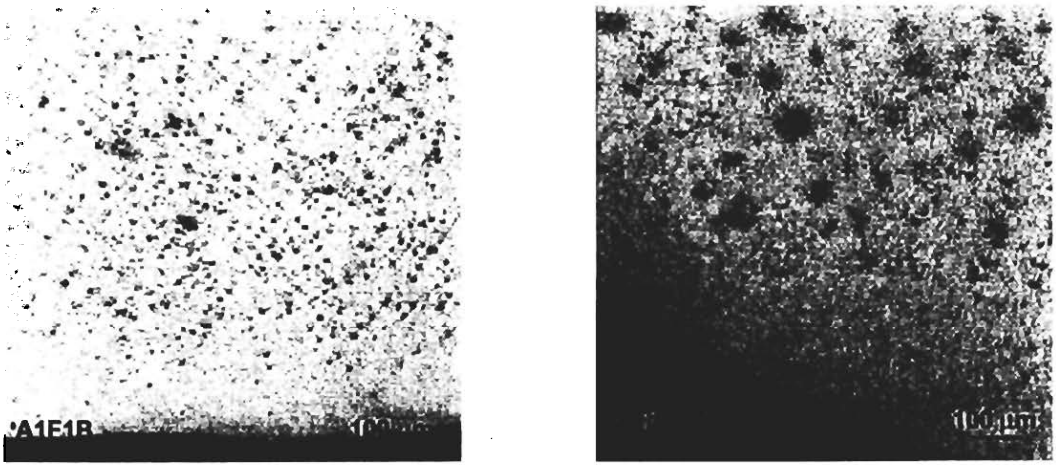

a) b)

**Figure 32** Optical micrographs of A1F1 edge a) as-polished and b) etched

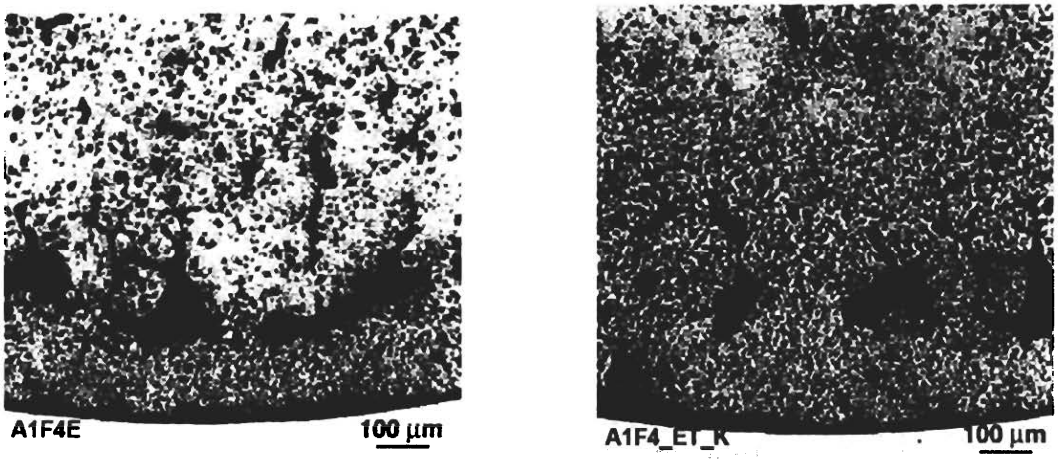


a) b)

**Figure 33** Optical micrographs of A1F4 edge a) as-polished and b) etched

Comparisons between the AFC-1B and AFC-1F transmutation metallic alloy fuels and U-xPu-10Zr fuels show similar microscopic and swelling characteristics at equivalent fission density. The U-xPu-10Zr metallic alloy fuels exhibit three stages of porosity development and swelling: 1. incubation characterized by very low swelling rate up to a threshold burnup of ~3.5 x $10^{20}$ f/cm$^3$ (1.0 at.% U-xPu-10Zr), 2. transition characterized by rapid fission gas driven swelling until a network of open porosity fully develops, the fuel contacts the cladding and majority of fission gas is released occurring at burnups between ~3.5 – 10 x $10^{20}$ f/cm$^3$ (1.0-3.0 at.% U-xPu-10Zr) and 3. stable irradiation change characterized by a slowly increasing plateau due to accumulation of solid fission products and retained fission gas occurring at burnups > 10 x $10^{20}$ f/cm$^3$ (3.0 at.% U-xPu-10Zr) [Ref. 8]

The differences in the microstructural evolution of both non-fertile and fertile metallic alloys is explained directly as the difference in irradiation damage (indicated by fission density) and is independent of the specific composition. The five specimens that exhibit significant radial swelling have the highest fission damage (measured by fission density). The transition stage of rapid swelling for the transmutation metallic fuels begins between 5.0 and 5.9 x $10^{20}$ f/cm$^3$. Fortuitiously, the fission density of the transmutation metallic fuels are in the late incubation and early transition stages of porosity development and swelling, thus providing data to evaluate the transition stage of transmutation compositions. The observation of the transition behavior being similar to U-xPu-10Zr fuels provides another indication that the fuel performance of metallic fuel forms is similar for a wide range of actinide compositions and zirconium content.

### 4.8 Metallic Alloy Isotopic and Burnup Analyses

Isotopic and burnup analyses were performed on eleven metallic transmutation fuel specimens. There are five non-fertile specimens from Experiment AFC-1B and six fertile metallic alloys samples from Experiment AFC-1F.

The burnup of AFC-1B and AFC-1F specimens was determined from the measured plutonium-239 and uranium-235 atoms (HM) and the derived number of fissions (F.P.), based on a measured fission product and its fission yield. The resulting expression is

$$\text{Burnup (GWd/tHM)} = [\text{F.P.} / (\text{F.P.} + \text{HM})] \times 100\% \text{ at.\%}$$

Figures 34 and 35 summarize the burnup measurements of AFC-1B and AFC-1F specimens for different burnup monitor isotopes. The burnup monitor isotopes were selected as candidates based on the following properties: 1. it is stable or long-lived, 2. it has a yield greater than 1%, 3. the yield is similar for $^{235}$U and $^{239}$Pu and insensitive to neutron spectrum and 4. it is not mobile in the fuel matrix. $^{148}$Nd is used as the burnup monitor in the standard method for oxide fuel burnup analysis, but it requires a chemical separation process and a correction due to absorption of $^{147}$Nd. Because of the short analysis time for ICP-MS, many isotopes can be measured in a relatively short amount of time, so it is possible that another monitor isotope or combination of monitor isotopes can provide an alternative method that is much less time consuming or more accurate.

The uncertainty of the results is ~15%. There is good agreement between the burnup monitors for each fuel specimen. The burnup values derived from isotopic analyses are somewhat lower than the calculated burnup values, but the difference is not statistically significant.

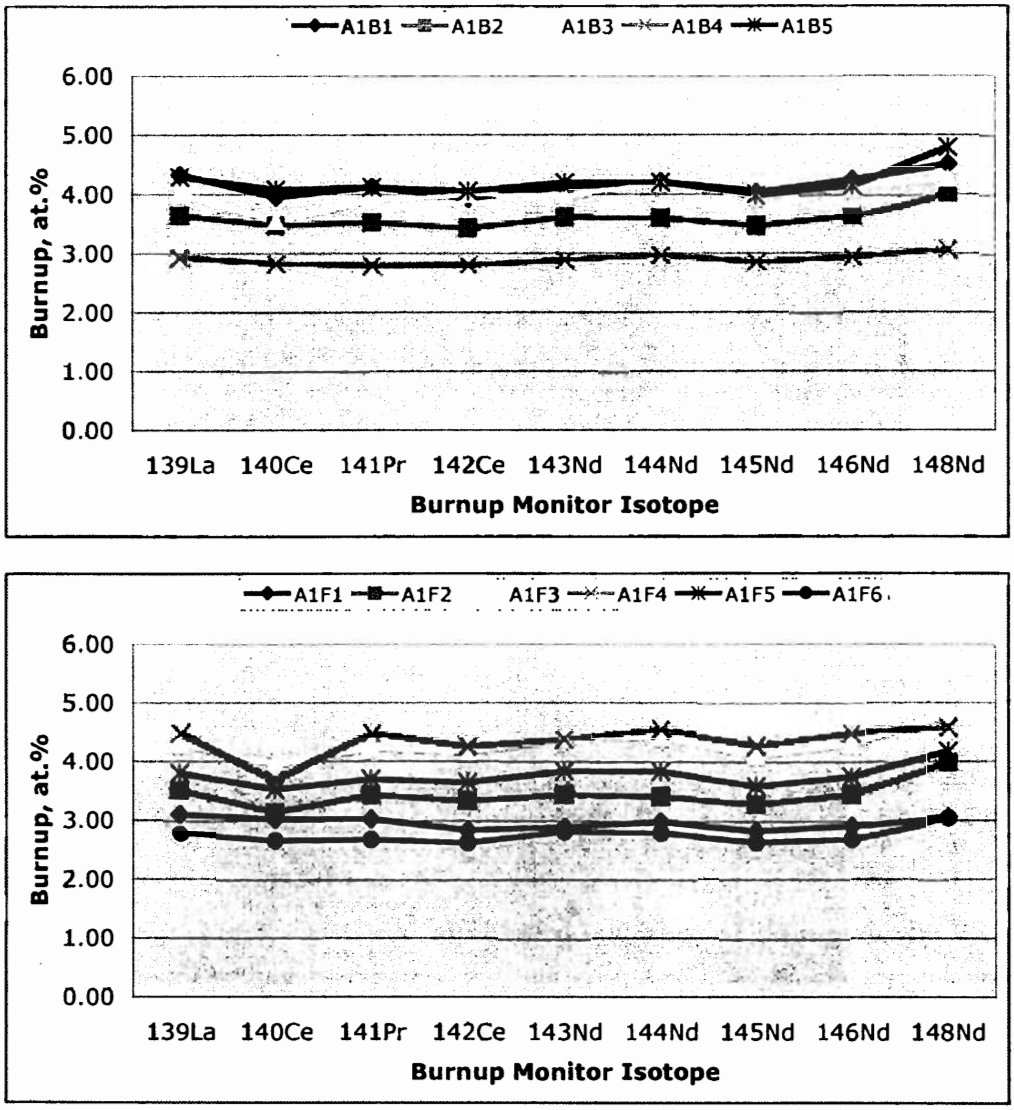


**Figure 34** Measured burnup of AFC-1B and AFC-1F derived from different burnup monitor isotopes

# 5 NITRIDE ALLOY TRANSMUTATION FUELS PIE

The preliminary results of post-irradiation hot cell examinations (PIE) of Experiment AFC-1Æ are presented in this section. PIE of these irradiation fuel experiments provides irradiation performance data for non-fertile and fertile actinide-bearing nitride fuel compositions at an intermediate burnup of 4-8 at%. Irradiation performance data of one of the compositions at burnup ~25-35 at.% will be obtained from a sibling experiment that is currently being irradiated at the INL ATR. The PIE of the 25-35 at.% burnup nitride sample is tentatively planned to begin in the first part of 2008.

These data support AFCI objectives to evaluate technical feasibility of nitride transmutation fuel forms. The PIE data also support transmutation fuel testing in the FUTURIX-FTA irradiation experiment currently scheduled to commence in 2007.

## 5.1 Nitride Rodlet Visual Examination

After unloading, the five nitride rodlet assemblies were visually examined to identify deviations from the as-built condition, such as cladding tube and end cap failures, deformations, cracks, blisters, areas of discoloration, corrosion, and loss of material by wear. The visual examinations revealed no such deviations. Fig. 35 shows the digital still photographs of Rodlets A1Æ1 and A1Æ6, typical of the five nitride fuel rodlets.

a) b)

**Figure 35** Visual examination digital still photographs of transmutation nitride fuel rodlet assemblies a) A1Æ1 with $(Pu_{0.5}Am_{0.5})N$-36ZrN fuel composition and b) A1Æ6 with $(U_{0.5}Pu_{0.25}Am_{0.15}Np_{0.10})N$ fuel composition

## 5.2 Nitride Rodlet Assembly Dimensional Inspections

Dimensional inspection of AFC-1AE Irradiation Test rodlets is summarized in this section. Five nitride rodlets and one dummy rodlet from AFC-1AE Capsule were inspected by INL Element Contact Profilometer (ECP). Four diameter profiles separated 45 degrees apart were measured at 0.1 in. axial intervals (2.54 mm). The accuracy is ±0.0003 in. (7.6 $\mu$m). The results indicate that the rodlets' nominal diameter is the same as the as-built dimension. There were however differences displayed on some of the profiles attributed to effects of the disassembly milling.

The diameter profile of some of the rodlets exhibited localized burrs or reduced wall thickness, both being effects of the disassembly milling operation. The localized burrs (localized points) ranged from 0.001 – 0.004 in. in height and spanned 0.1-0.3 in. Figure 36 shows an example of a rodlet with nominal diameter and one small burr at 1.6 in. axial position. There were other profiles that revealed a decrease in wall thickness, which was indicated by a slowly decreasing diameter profile. Fig. 37 shows a diameter profile of A1Æ3 (NN-4A) displaying cladding wall thickness reduction due to disassembly milling operation.

The mass of the nitride fuel rodlet assemblies was measured after capsule disassembly. Table 5 displays the as-built and postirradiation mass of each rodlet. There are slight differences in some of the rodlets which are attributed to the loss of cladding material that occurred during disassembly milling operation. A1Æ3 (NN-4A) exhibited the largest difference in mass. This is explained by an additional disassembly step that was attempted with this rodlet prior to disassembly milling. A part of the upper and lower endcaps were sectioned to facilitate removal by the Push Tool, however this was unsuccessful and A1Æ3 was removed by disassembly milling. The mass of the two sectioned endcap pieces is ~0.7 g, which is about the magnitude of the difference of the as-built and PIE mass. Additional mass loss would be attributed to milling. In conclusion, results of the mass measurement are not definitive because of the effects of the disassembly process, but comparisons of the as-built and postirradiated mass suggest that there were no fuel failures.

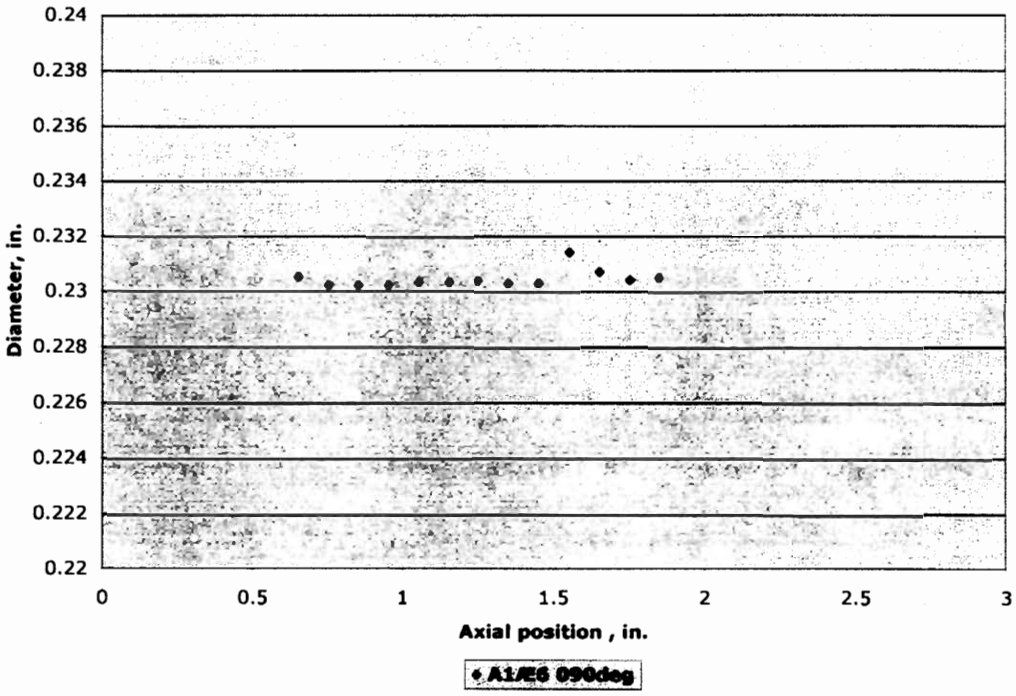


**Figure 36** Diameter profile of A1Æ6, $(U_{0.5}Pu_{0.25}Am_{0.15}Np_{0.10})N$, sample irradiated to 5.8 x $10^{20}$ f/cm$^3$ (4.6 at.%) burnup. Example of localized burr effect due to disassembly milling operation (see isolated point at 1.6 in. axial position)

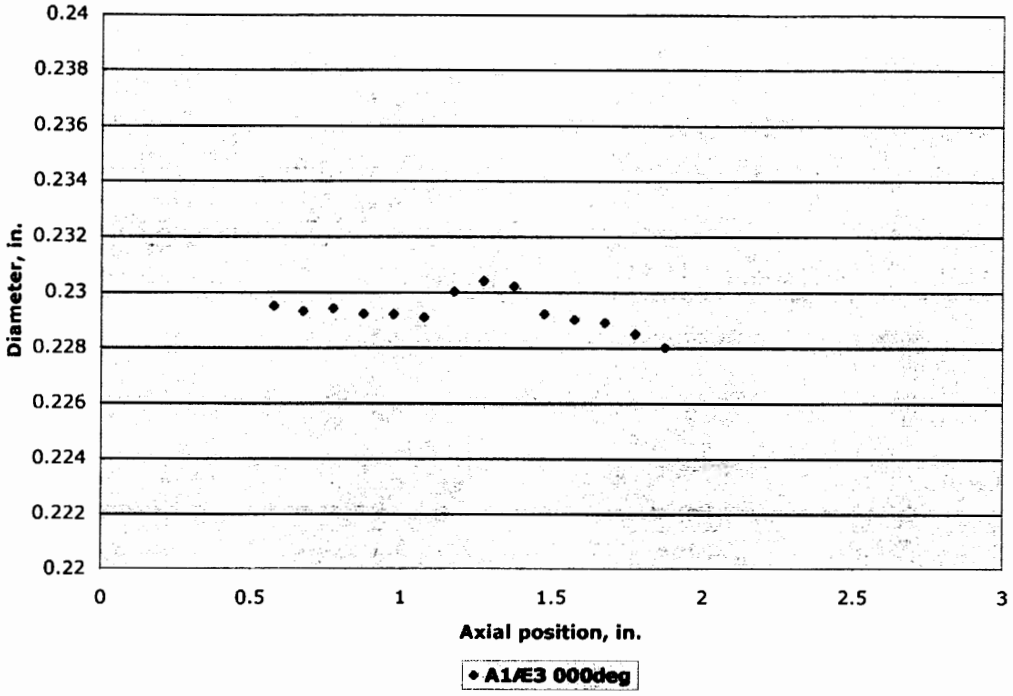


**Figure 37** Diameter profile of A1Æ3, $(Pu_{0.5}Am_{0.5})N$-36ZrN, irradiated to 3.5 x $10^{20}$ f/cm$^3$ (7.5 at.%) burnup. Example of cladding wall reduction due to disassembly milling operation (compare profile to as-built diameter of 0.230 in.)

**Table 5 Mass of AFC-1Æ Nitride Rodlets**

| Rodlet | Mass As-Built, g | Mass PIE, g | Difference[a], g |
|---|---|---|---|
| **AFC-1AE Rodlets** | (±0.01) | (±0.001) | (±0.01) |
| A1Æ1 (NN-1B) | 17.09 | 16.944 | -0.146 |
| A1Æ2 (DUM-1AE) | 19.44 | 19.439 | +0.006 |
| A1Æ3 (NN-1B) | 17.52 | 16.743 | -0.777[b] |
| A1Æ4 (NN-1Aa) | 13.24 | 12.935 | -0.305 |
| A1Æ5 (NM-1A) | 17.09 | 16.944 | -0.146 |
| A1Æ6 (LNX-4Ba) | 19.44 | 19.439 | -0.001 |
| | | | |

a Disassembly milling operation removed some cladding material as evidenced by diameter profiles. The potential decrease in mass was not quantified.
b A part of the upper and lower endcaps (~0.7g mass) were sectioned from Rodlet 3 as part of disassembly process before PIE mass was measured

## 5.3 Nitride Rodlet Neutron Radiography

Rodlet neutron radiography was performed on five nitride and one dummy irradiated in the AFC-1Æ capsule. Figure 38 shows rodlet neutron radiography of AFC-1Æ. AFC-1Æ Capsule comprised both non-fertile and low-fertile nitride transmutation fuel forms (see Sec. 2 for compositions).

The compositions to be tested in the FUTURIX-FTA Irradiation Test are $(Pu_{0.5}Am_{0.5})N$-36ZrN and $(U_{0.5}Pu_{0.25}Am_{0.15}Np_{0.10})N$. A1Æ1 and A1Æ3 contain $(Pu_{0.5}Am_{0.5})N$-36ZrN samples fabricated by the process planned for the FUTURIX-FTA tests. A1Æ4 contains $(Pu_{0.5}Am_{0.5})N$-36ZrN composition, but was fabricated in an earlier campaign by a different process than that proposed for FUTURIX-FTA samples. A1Æ6 contains the low-fertile $(U_{0.5}Pu_{0.25}Am_{0.15}Np_{0.10})N$ composition planned for the FUTURIX-FTA tests.

As was the case for the metallic alloy rodlets, four of the nitride rodlets were inverted during disassembly and in-cell storage. The inverted rodlets were A1Æ3, $(Pu_{0.5}Am_{0.5})N$-36ZrN (HB)), A1Æ4, $(Pu_{0.5}Am_{0.5})N$-36ZrN non-FUTURIX), A1Æ5, $(Pu_{0.5}Am_{0.25}Np_{0.25})N$-36ZrN) and A1Æ6, $(U_{0.5}Pu_{0.25}Am_{0.15}Np_{0.10})N$). Two of the four rodlets that were inverted exhibited axial relocation of the fuel column (A1Æ3 and A1Æ6), however the other two- A1Æ4 and A1Æ5- did not exhibit any obvious effects from being inverted. In order to understand the relocation behavior, the fabrication, irradiation, and disassembly history of these rodlets is discussed.

**Figure 38** Rodlet neutron radiography of AFC-1Æ non-fertile and low-fertile nitride Rodlets from l. to r. A1Æ1, A1Æ2, A1Æ3, A1Æ4, A1Æ5 and A1Æ6

Figures 39 and 40 display the fuel condition of the inverted nitride rodlets in chronological sequence from as-built x-ray radiography, hot cell receipt neutron radiography and disassembled rodlet neutron radiography. Figure 39 shows the two nitride rodlets (A1Æ4 and A1Æ5) that were inverted, but did not exhibit relocation and Figure 40 shows the two nitride rodlets (A1Æ3 and A1Æ6) that were inverted and did exhibit relocation. The fuel condition seen in the as-built x-ray radiographs and hot cell receipt neutron radiographs show significant differences in the fuel pellets that exhibit axial relocation. In the as-built condition, A1Æ6 (Figure 40a) and A1Æ3 (Figure 40d) show a greater amount of fragmentation (seen as fragments collected around the lower endcap) than appears on the A1Æ4 (Figure 39a)and A1Æ5 (Figure 39d) radiographs. A1Æ6 and A1Æ3 also show significant cracking and fragmentation in the hot cell receipt radiographs (Figure 40b,e), which is prior to any disassembly operations. Rodlets A1Æ4 and A1Æ5, in contrast, do not show any indication of cracking and fragmentation in the hot cell receipt radiographs (Figure 39b,e).

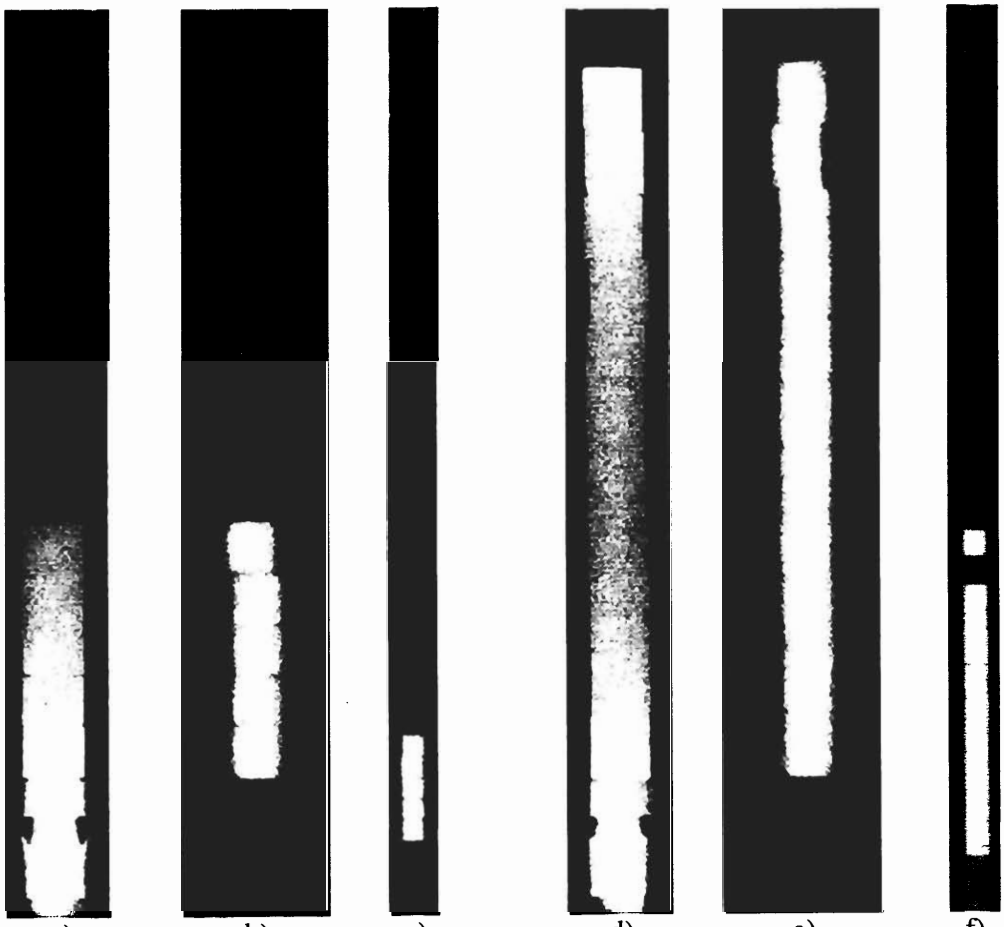


**Figure 39** Radiography of nitride rodlets that were inverted and did not exhibit axial relocation a) A1Æ4 as-built, b) A1Æ4 hot cell receipt, c) A1Æ4 after disassembly milling operation, d) A1Æ5 as-built, e) A1Æ5 hot cell receipt, f) A1Æ5 after disassembly milling operation

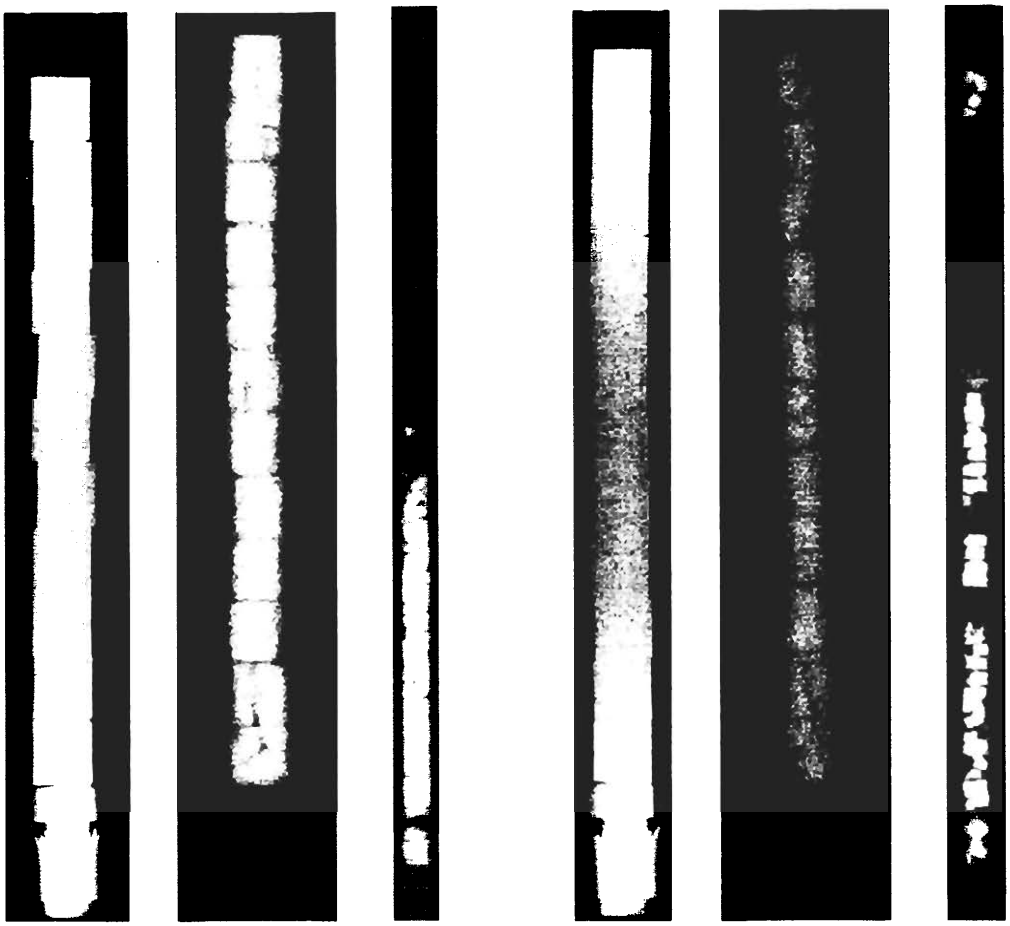


**Figure 40** Radiography of nitride rodlets that were inverted and exhibit axial relocation a) A1Æ6 as-built, b) A1Æ6 hot cell receipt, c) A1Æ6 after disassembly with Push Rod, d) A1Æ3 as-built, e) A1Æ3 hot cell receipt, f) A1Æ3 after disassembly milling operation

The major observations of nitride fuel axial relocation in A1Æ3 and A1Æ6 are summarized:

1. A1Æ3 and A1Æ6 showed more evidence of fragmentation in the as-built condition than A1Æ4 and A1Æ5
2. Only A1Æ3 and A1Æ6 showed radial relocation (cracking and fragmentation) postirradiation at initial receipt in hot cell
3. A1Æ3 and A1Æ6 accumulated the highest fission density of the nitride rodlets (approximately 5-25% higher than A1Æ4 and A1Æ5)

An explanation of nitride fuel axial relocation should also incorporate the following observations from the other PIE examinations

- 4 metal and 4 nitride rodlets were inverted during disassembly operations
- 2 of the 4 nitride rodlets, A1Æ3 and A1Æ6, exhibited axial relocation and none of the metallic alloy rodlets
- There were no fuel cladding failures, so there is no potential for oxidant (oxygen, moisture) intrusion in rodlet atmosphere to cause degradation
- Sodium bond material remains contained within rodlet (specific location undetermined)

The current conclusions of nitride fuel axial relocation in A1Æ3 and A1Æ6 are summarized:

1. No axial relocation occurred during irradiation.
2. The combination of pre-existing flaws and incipient cracks in the as-built condition and the slightly higher burnup of A1Æ3 and A1Æ6 resulted in relocation (radial and axial when inverted).
3. Radial relocation is an expected behavior of all irradiated nitride fuel after reaching specified burnup threshold. (N.B. the burnup threshold is expected to depend on fragmentation susceptibility in as-built condition so is likely to be higher than A1Æ3 and A1Æ6).
4. Axial relocation is possible in nitride fuels that exhibit radial relocation and is predicted if rodlets are inverted.
5. The sodium bond does not prevent relocation, at least for low swelling and highly fragmented fuel

### 5.4 Nitride Rodlet Gamma Scan

Gamma scan analyses of AFC-1Æ Irradiation Test rodlets are summarized in this section. Five nitride rodlets and one dummy rodlet were analyzed for the following fission products (Cs-134, Cs-137, Nb-95, Pr-144, Rh-106m, Ru-103, Zr-95) and activation products (Co-60, Mn-54). Figures 41-42 show the gamma scan results for three of the rodlets A1Æ1, A1Æ3 and A1Æ6 as being prototypic of the AFC-1Æ nitride fuel specimens. At the top of each gamma scan graph is the neutron radiograph image to facilitate comparison between the fission product activity axial profile and internal rodlet features. The cross-sectional metallography is also shown for comparison with radial swelling and microstructural featuares. The significance of the four isotopes displayed is primarily for comparison with the metallic fuel gamma scans and secondly as representative of different fission product categories: 1. Nb-95 and Ru-103 noble metals, 2. Pr-144 a rare earth, and 3. Cs-137 an alkali metal that dissolves to some extent in the bond sodium. Some general observations for all the nitride rodlets are provided. First, all the fission products, including cesium, map with the fuel location irrespective of the nitride alloy composition and burnup in the range of $2.7 - 4.5 \times 10^{20}$ f/cm$^3$. Second, in the rodlets with fuel relocation, the lower activity positions correspond to physical features such as pellet-to-pellet interfaces, fuel fragments or gaps in the fuel column. Third, the relative activity of the rodlets corresponds approximately to the relative fission density.

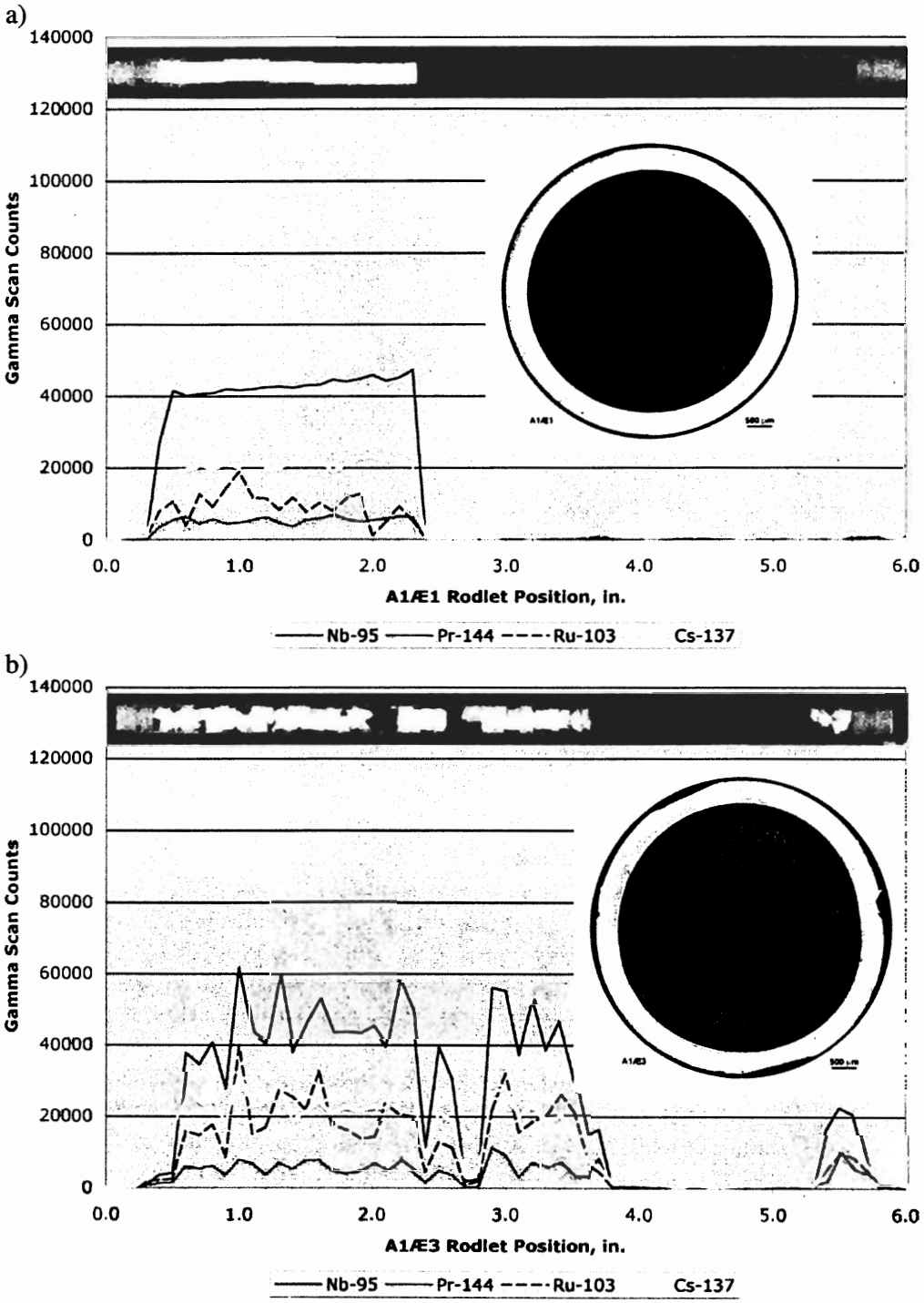


**Figure 41** Gamma scan analysis of $(Pu_{0.5}Am_{0.5})$N-36ZrN samples a) A1Æ1 irradiated to 2.7 x $10^{20}$ f/cm$^3$ (5.1 at.%) burnup and b) A1Æ3 irradiated to 3.5 x $10^{20}$ f/cm$^3$ (7.5 at.%) burnup

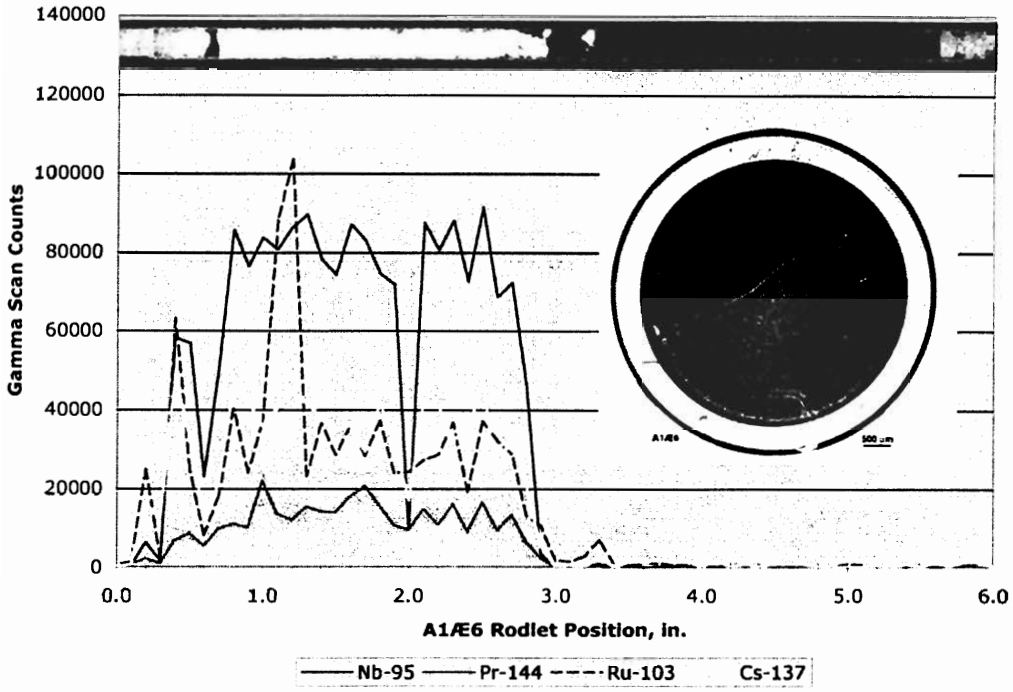


**Figure 42** Gamma scan analysis of $(U_{0.5}Pu_{0.25}Am_{0.15}Np_{0.10})N$ sample A1Æ6 irradiated to 4.5 x $10^{20}$ f/cm$^3$ (4.6 at.%) burnup

## 5.5 Nitride Rodlet Fission Gas Puncture and Analyses

Fission gas samples were collected from the five nitride rodlet assemblies from AFC-1Æ irradiation tests using the GASR laser puncturing and gas sampling system. The rodlet gas samples were analyzed for elemental and isotopic composition by gas mass spectrometry. Comparison of the elemental composition with as-built fill gas composition verified that there were no rodlet failures. This confirmed conclusions of the visual and dimensional inspection results.

Fission gas and fractional helium release values were determined for each sample. The fission gas release was derived from the postirradiation and as-built elemental gas composition, the as-built rodlet internal void volume and internal gas pressure, and the fuel burnup. The fractional helium release was derived similarly from the postirradiation helium content, the as-built characterization data and the helium generation during irradiation. Helium generation was estimated to come only from americium transmutation.

Figure 43 displays the fission gas release and helium burnup dependence of the 5 nitride rodlets. The fission gas and helium release shows a threshold burnup dependence with no release below 2.7 x $10^{20}$ f/cm$^3$. Above the burnup threshold, fission gas release ranges between 7 and 214%. The one nitride composition with uranium A1Æ6 has the highest burnup, but shows moderate release of 10%. This may indicate lower fission gas release from low-fertile compositions compared to non-fertile compositions. The helium gas release trends with fission gas release, but is slightly lower similar to the metallic alloy fuel behavior.

Figure 44 displays the axial growth, helium release and fission gas release for the AFC-1Æ specimens. It is evident that all three parameters trend together, however there is very little axial growth, with the peak being less than 2%.

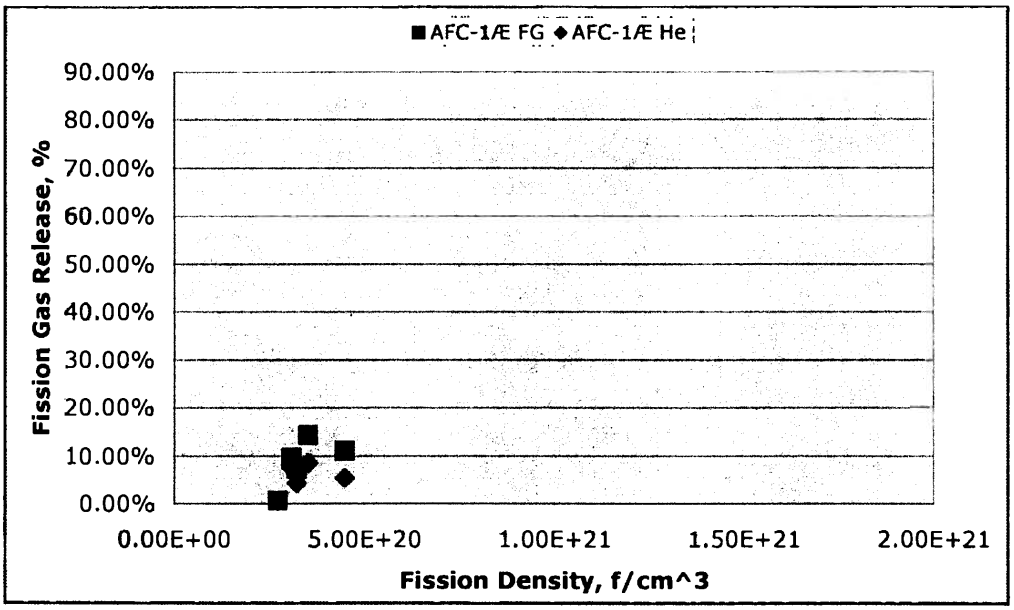


**Figure 43** Fission gas and helium release dependence on fission density for nitride transmutation fuel rodlets irradiated in AFC-1Æ Capsule

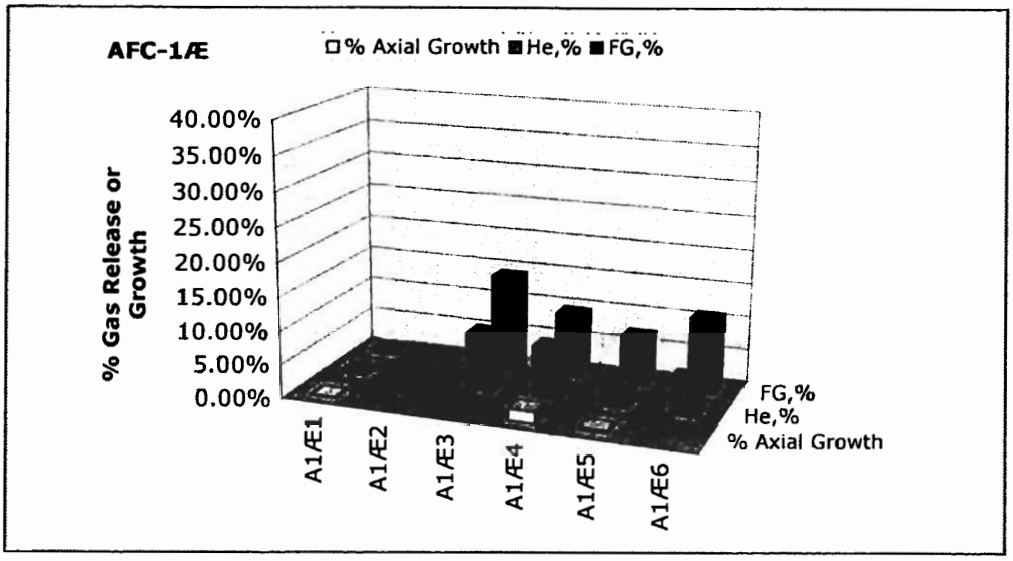


**Figure 44** Axial growth, helium release and fission gas from nitride transmutation fuel rodlets irradiated in AFC-1Æ Capsule

## 5.6 Nitride Rodlet Sectioning

Cross-sectional (transverse) samples for isotopic and burnup analyses and metallography were sectioned from all AFC-1Æ Rodlets. The sectioning location of the isotopic samples was 0.25 – 0.50 in. from the bottom of the rodlets and the sectioning location of the metallography samples was 0.50 – 0.75 in. from the bottom of the rodlets.

## 5.7 Nitride Ceramography

Ceramography results of all five AFC-1Æ nitride samples are presented. There are four non-fertile and one fertile nitride specimens. A1Æ1, A1Æ3 and A1Æ6 specimens are the compositions that are planned for testing in the FUTURIX-FTA Irradiation Test. A1Æ4 has the $(Pu_{0.5}Am_{0.5})$N-36ZrN FUTURIX-FTA composition, but was fabricated by a different method. The actinide nitrides were formed first from oxide feedstock then mixed and sintered, whereas the FUTURIX-FTA composition followed the traditional fabrication route of mixing the actinide oxides and then nitridization together to form a mixed-nitride solid solution. Montage (or composite) overviews of the transverse cross sections were created from 12-16 images taken at 5X objective magnification. Detailed ceramography was performed at magnifications up to ~500X. There were some samples that exhibited slight rounding at the highest magnification.

Figure 45 shows the cross-sectional ceramography of the AFC-1Æ specimens as-polished. All nitride specimens exhibited some areal swelling. A1Æ1, which has the lowest fission density, exhibits the least areal swelling and no cracking or fragmentation, which is termed relocation. Four of the five nitride specimens (A1Æ3, A1Æ4, A1Æ5 and A1Æ6) exhibited slight areal swelling and measurable relocation. These four specimens all exhibited a radial crack that propagated through the edge.

In A1Æ3, there is a fragment shard that would likely have caused premature failure in a helium bonded rod. The sodium bond ameliorates susceptibility to fragment induced failures because of its much higher thermal conductivity, which will reduce the peak temperature (local hot spot) at the small fragment. However, this type of fragment may lead to failures at higher burnup.

Figures 46-47 show optical micrographs of A1Æ1 as-polished interior and edge regions. The interior shows a homogenous multiphase mixture with some agglomerates 100 $\mu$m x 200 $\mu$m and finely distributed porosity with some larger acicular pores. The nitrides exhibit a 50-100 $\mu$m rim different than the interior microstructure. Interestingly, the metallic transmutation fuels also exhibit a rim, however the nitride rim spatial dimension is somewhat less than observed in metallic fuel. Figure 46 shows a higher magnification of an agglomerate in A1Æ1 interior. A color enhanced image is juxtapose the grey balanced micrograph to compare the distribution of contrast regions in the agglomerate and the matrix. The agglomerate is on the left of the pore and the matrix on the right. The agglomerate has much less of the light green areas, which are adjacent to the dark green pore regions.

Figure 48 shows optical micrographs of A1Æ3 as-polished interior and edge regions. Higher magnification micrographs of A1Æ3 interior are shown in Figure 49. A1Æ3 shows a homogeneous microstructure and finely distributed porosity. There are lighter contrast agglomerates, but somewhat smaller size compared to A1Æ1. The higher magnification micrographs indicate some areas of different composition or density. Similar features are observed in A1Æ5 and A1Æ4.

The microstructure of A1Æ6 interior and edge regions are shown in Figure 50. A1Æ6 has a homogeneous multiphase microstructure and distribution of fine pores. There does not appear to be agglomerate regions as observed in the non-fertile compositions, but perhaps they are smaller scale. A rim with different contrast is evident in the cross-section montage, but not so clearly in the high magnification image.

In conclusion, the difference in fuel behavior correlates with the burnup (i.e., fission density). The nitride ceramography results also underscore the importance of using fission density rather than at.% as the burnup metric for correlating fuel performance. Based on at.%, A1Æ1 has 5.1 at.% burnup compared to 4.6 at.% depletion for A1Æ6, however A1Æ1 has less areal swelling and fission gas release which should trend upward with irradiation damage. Based on fission density, A1Æ1 sample has 2.7 x $10^{20}$ f/cm$^3$ compared to 4.5 x $10^{20}$ f/cm$^3$ for A1Æ6.

Relocation is commonly observed in irradiated nitrides as is the case for the ceramic fuel forms such as oxides and carbides [Ref. 14, 15]. However, cracking is generally pie shaped fragments rather than a through diameter crack. This cracking morphology may be due to high residual stresses causesd during fabrication. The endcapping and fragmentation observed during fabrication is evidence of high residual internal stresses probably generated during the pressing step. Using fission density, the swelling and relocation behavior of the nitride transmutation fuel is explainable with a consistent mechanism. In comparison with the very limited data for mixed nitride irradiation behavior, particularly with Na bond, the transmutation compositions appear to behave similarly.

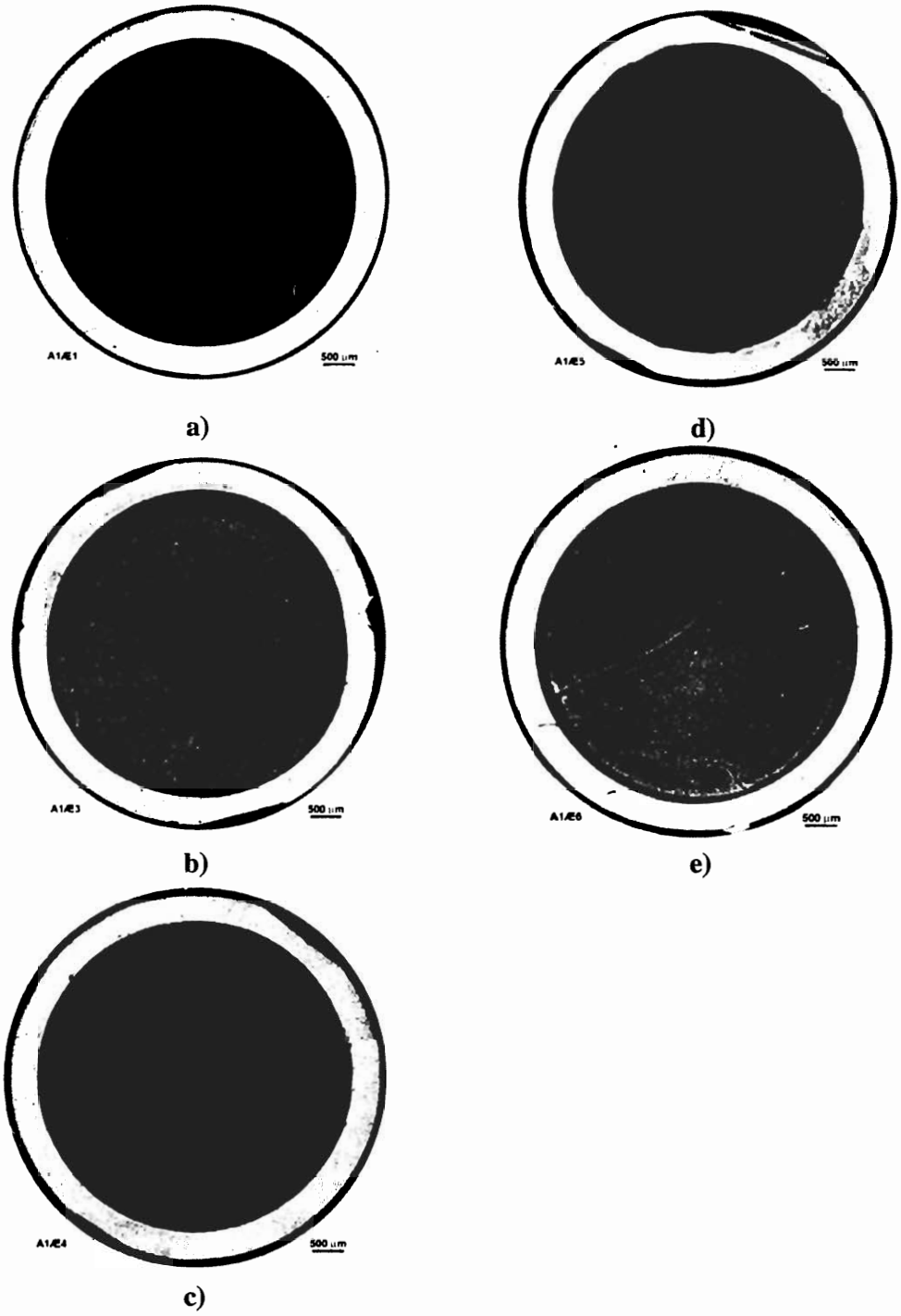


**Figure 45** Cross-sectional metallography of AFC-1Æ nitride samples a) A1Æ1 irradiated to 2.7 x $10^{20}$ f/cm$^3$ (5.1 at.%), b) A1Æ3 irradiated to 3.5 x $10^{20}$ f/cm$^3$ (7.5 at.%), c) A1B4 irradiated to 3.1 x $10^{20}$ f/cm$^3$ (7.8 at.%) d) A1Æ5 irradiated to 3.2 x $10^{20}$ f/cm$^3$ (7.5 at.%) and e) A1Æ6 irradiated to 4.5 x $10^{20}$ f/cm$^3$ (4.6 at.%)

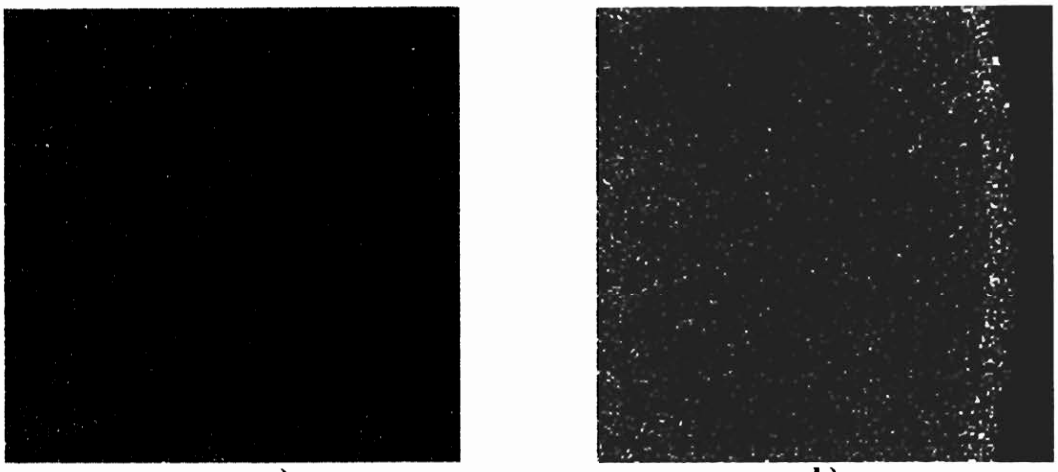

a) b)

**Figure 46** Optical micrographs of A1Æ1 as-polished a) interior and b) edge region

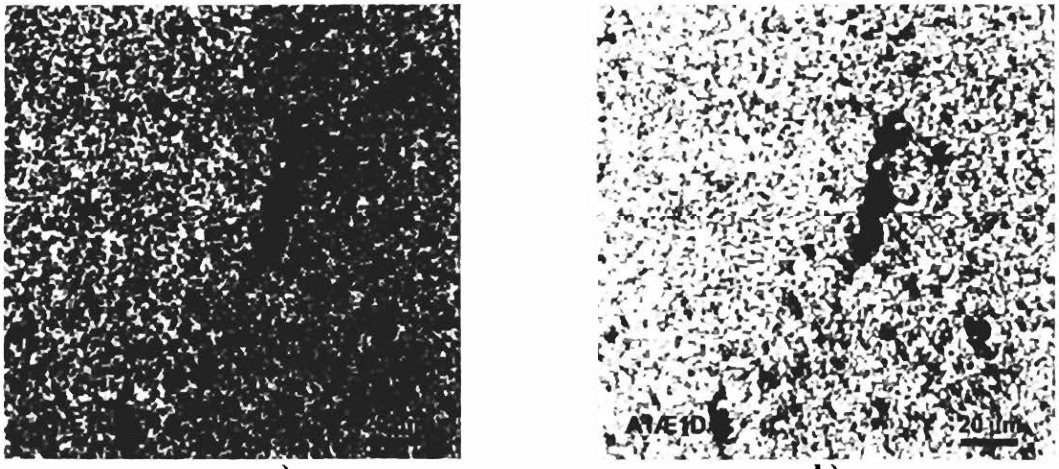


a) b)

**Figure 47** Higher magnification micrograph of A1Æ1 interior showing agglomerate and matrix a) grey balanced color and b) color enhanced to contrast areas of varying light reflectivity

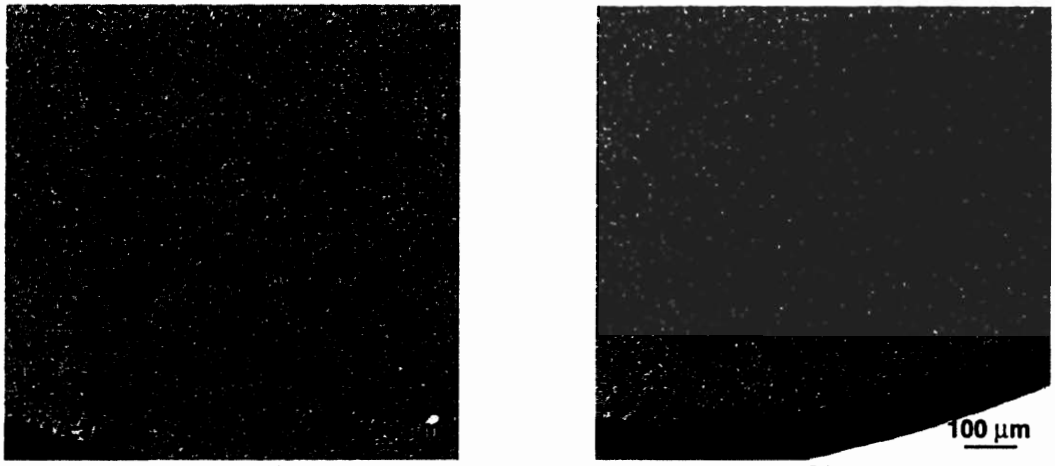


a) b)

**Figure 48** Optical micrographs of A1Æ3 as-polished a) interior and b) edge region

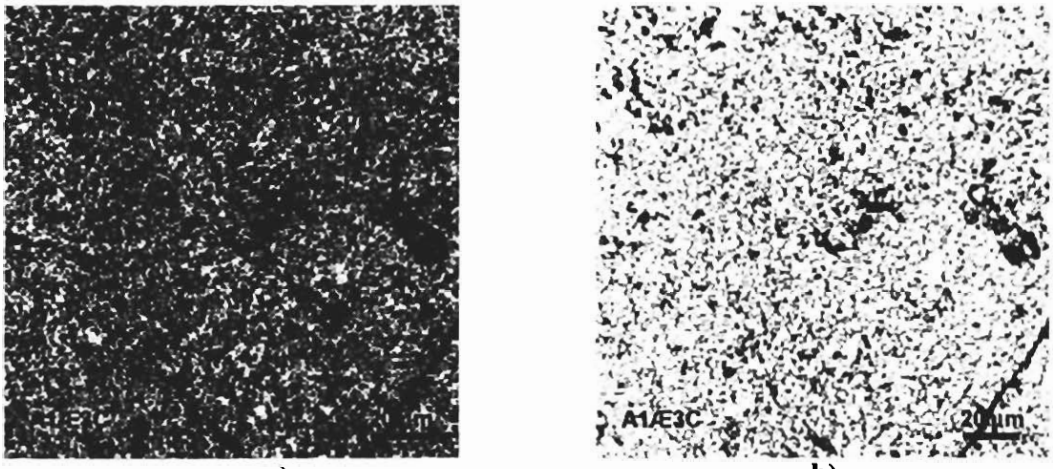


a) b)

**Figure 49** Higher magnification micrograph of A1Æ3 interior a) grey balanced color and b) color enhanced to contrast areas of varying light reflectivity

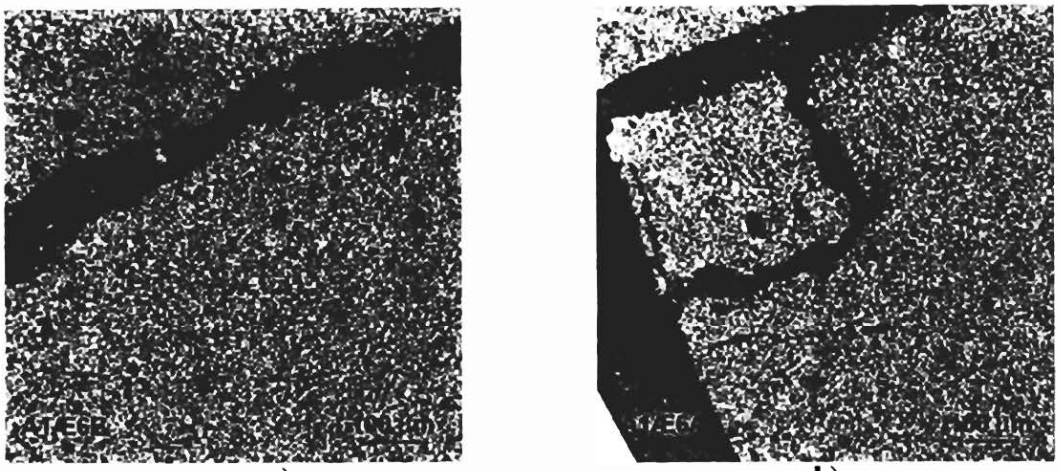

a) b)

**Figure 50** Optical micrographs of A1Æ6 as-polished a) interior and b) edge region

## 5.8 Nitride Isotopic and Burnup Analyses

Isotopic and burnup analyses were performed on five nitride transmutation fuel specimens. There are four non-fertile and one fertile specimens from Experiment AFC-1Æ.

The burnup was determined from the measured plutonium-239 and uranium-235 atoms (HM) and the derived number of fissions (F.P.), based on a measured fission product and its fission yield. The resulting expression is

Burnup (GWd/tHM) = [F.P. / (F.P. + HM)] x 100% at.%

Figure 51 summarizes the burnup measurements of AFC-1Æ specimens for different burnup monitor isotopes. The burnup monitor isotopes were selected as candidates based on the following properties: 1. it is stable or long-lived, 2. it has a yield greater than 1%, 3. the yield is similar for $^{235}U$ and $^{239}Pu$ and insensitive to neutron spectrum and 4. it is not mobile in the fuel matrix. $^{148}Nd$ is used as the burnup monitor in the standard method for oxide fuel burnup analysis, but it requires a chemical separation process and a correction due to absorption of $^{147}Nd$. Because of the short analysis time for ICP-MS, many isotopes can be measured in a relatively short amount of time, so it is possible that another monitor isotope or combination of monitor isotopes can provide an alternative method that is much less time consuming or more accurate.

The uncertainty of the results is ~15%. There is good agreement between the burnup monitors for each fuel specimen. In general, the burnup monitor neodymium-148 results in a slightly higher derived at.% burnup. The neodymium monitors were not reported for A1Æ3 due to a question of sample integrity. The Nd isotopes were analyzed a few months after the other analytes and the solution had degraded during storage in the hot cell. The burnup values derived from isotopic analyses are somewhat lower than the calculated burnup values, but the difference is not statistically significant.

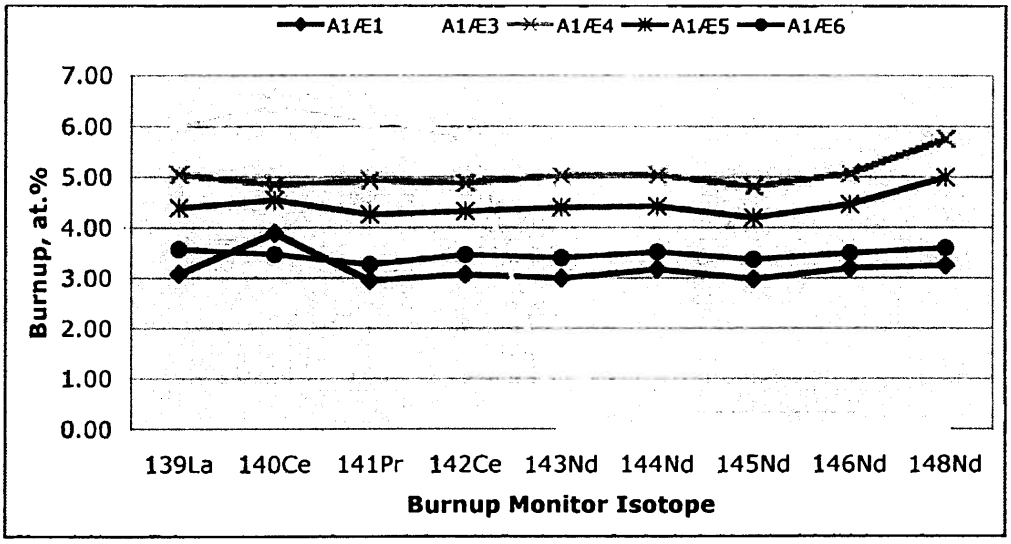


**Figure 51** Measured burnup of AFC-1Æ nitride transmutation fuel specimens derived from different burnup monitor isotopes

# 6 SUMMARY

Postirradiation hot cell examinations of AFC-1 irradiation tests was completed for eleven metallic alloy transmutation fuel rodlets and five nitride transmutation fuel rodlets. The rodlets compositions included non-fertile (i.e., no uranium) and low-fertile (i.e., uranium bearing) fuel samples. Non-destructive exams including visual examination, dimensional inspection, gamma scan analysis, and neutron radiography were performed on the eleven metallic alloy and five nitride rodlets. Detailed examinations including fission gas puncture and analysis, metallography / ceramography and isotopics and burnup analyses were performed on five metallic alloy and three nitride transmutation fuels. The conclusions are summarized below:

1. No rodlet failures were observed in the metallic and nitride fuel forms irradiated to 4-8 at.%.
2. Two burnup metrics are required to correlate data – at.% is most appropriate for measuring transmutation effectiveness and fission density is most appropriate for interpreting irradiation fuel performance.
3. Four metal and four nitride rodlets were inverted sometime during disassembly operations at INL hot cell. Inverting had no effect on the metallic alloy rodlets. Two of the four nitride rodlets exhibited axial relocation of fuel column after inverted
4. The irradiation behavior of metallic alloy transmutation fuel compositions is similar to that of U-xPu-10Zr when correlated to fission density.
5. The irradiation performance of the nitride fuel forms is comparable to the limited data available on mixed nitride fuel performance.

# 7 ACKNOWLEDGMENTS

The authors appreciate the significant contributions by J. Wiest and P. Lind, systems engineers for fuel examination stations in the Hot Fuels Examination Facility; L. C. Brauer, J. Colburn, J. Frye, S. Kahn, J. Kerr, B. Lundell, K. Runz, R. Scott, T. Tripp, S. White, and H. Houser of the Hot Fuels Examination Facility for non-destructive examinations and metallography. Additional support from D. Wahlquist and J. Blaylock for equipment development and engineering; and E. Franklin, R. Roesener and D. Darrington for coordinating transportation and shipping is appreciated. The authors appreciate A. Maddison, J. Berg, J. Fonnesbeck, D. Cummings, J. Giglio, C. Morgan, M. Huntley, M. Rodriguez, S. Wild, and M. Lambregts of the Analytical Laboratory for the fission gas, isotopics and burnup analyses. For metal fuel fabrication and characterization, the authors recognize R. Kennedy, M. Meyer, J. Stuart, B. Forsmann, J. Sommers, R. Fielding, R. Briggs, T. DeSanto, J. Cole and D. Keiser. S. Maloy, K. McClellan, S. Willson, and S. Voit of LANL are acknowledged for nitride fuel fabrication. The authors thank D. Utterbeck, G. Chang, R. Ambrosek, J. Williams, and R. Howard for irradiation testing coordination and safety analyses. J. Carmack and K. Pasamehmetoglu are recognized for technical and programmatic direction. The authors express appreciation to M. McCray of DOE-ID and F. Goldner of DOE-HQ for programmatic support.

# 8 REFERENCES


1. Report to Congress on Advanced Fuel Cycle Initiative: Objectives, Approach, and Technology Summary, U.S. Department of Energy Office of Nuclear Science and Technology, May 2005.
2. Report to Congress on Advanced Fuel Cycle Initiative: The Future Path for Advanced Spent Fuel Treatment and Transmutation Research, U.S. Department of Energy Office of Nuclear Science and Technology, January 2003.
3. S. L. Hayes, B. A. Hilton, M. K. Meyer, G. S. Chang, F. W. Ingram, S. Pillon, N. Schmidt, L. Leconte and D. Haas, "U. S. Test Plans for Actinide Transmutation Fuel Development," Trans. Am. Nucl. Soc., 87: 353, American Nuclear Society Winter Meeting, Washington, DC, 17-21 November 2002.
4. B. A. Hilton, S. L. Hayes, M. K. Meyer, D. C. Crawford, G. S. Chang, R. Ambrosek, "The AFC-1Æ and AFC-1F Irradiation Tests of Metallic and Nitride Fuels for Actinide Transmutation," Embedded Topical Meeting on Advanced Nuclear Energy Systems (GLOBAL 2003), New Orleans, Louisiana, 16-20 November 2003
5. S. L. Hayes, *Irradiation of Nitride and Metallic Fuels for Actinide Transmutation in the Advanced Test Reactor: Final Experiment Description and Design & Data Package for AFC-1A, AFC-1B, AFC-1C & AFC-1D*, ANL-W Document Control No. W7520-0481-ES-01, February 2003.
6. B. A. Hilton, *Irradiation of Nitride and Metallic Fuels for Actinide Transmutation in the Advanced Test Reactor: Final Experiment Description and Design & Data Package for AFC-1Æ & AFC-1F*, ANL-W Document Control No. W7520-0529-ES-01, July 2003.
7. B. A. Hilton, *Irradiation of Nitride and Metallic Fuels for Actinide Transmutation in the Advanced Test Reactor: Final Experiment Description and Design & Data Package for AFC-1G & AFC-1H*, INL Document Control No. W7520-0678-ES-01, May 2005.
8. G. L. Hofman, L. C. Walters and T. H. Bauer, "Metallic Fast Reactor Fuels", Prog. Nucl. Energy, Vol. 31, p. 83, 1997
9. D. L. Porter, Personal Communication, 2005.
10. R. G. Pahl, R. S. Wisner, M. C. Billone and G. L. Hofman, Proc. Int. Fast Reactor Safety Meeting, Snowbird, 1990, vol. IV (ANS, LaGrange Park, IL, 1990) p. 129.
11. D. L. Porter, C. E. Lahm and R. G. Pahl, "Fuel Constituent Redistribution during the Early Stages of U-Pu-Zr Irradiation", Metall. Trans. A, 1990, Vol. 21A, p. 1871.
12. R. G. Pahl, D. L. Porter, C. E. Lahm and G. L. Hofman, "Experimental Studies of U-Pu-Zr Fast Reactor Fuel Pins in the Experimental Breeder Reactor-II", Metall. Trans. A, 1990, Vol. 21A, p. 1863.
13. J. I. Cole, "AFCI Futurix-FTA Cast Fuel SEM Microstructure Characterization", Intra-Laboratory Memorandum, Idaho National Laboratory, 2006
14. Hj. Matzke, Science of Advanced LMFBR Fuels, North-Holland Physics Publishing, New York, 1986
15. H. Blank, Nonoxide Ceramic Nuclear Fuels in Materials Science and Technology, Vol. 10 Nuclear Materials, ed. B. Frost, VCH Publishers Inc., New York, 1994